Study of V_2O_5-GNPs Nanocomposites as a Promising Electrode Material for Supercapacitors Applications

By

Muhammad Oneeb

Supervised by

Prof. Javed Iqbal Saggu

Laboratory of Nanoscience and Technology (LNT)

Department of Physics, Quaid-i-Azam University

Islamabad

2023

This work is submitted as a dissertation in partial fulfillment of the requirement for the degree of

MASTER OF PHILOSOPHY

IN

PHYSICS

To The

Department of Physics
Quaid-i-Azam University Islamabad, Pakistan
2023

CERTIFICATE

This is to certify that the thesis entitled "**Study of V_2O_5-GNPs Nanocomposites as a Promising Electrode Material for Supercapacitors Applications"** by Muhammad Oneeb submitted to Quaid-I-Azam University, Islamabad for the degree of Master of Philosophy (M.Phil.) in Physics is a record of bonafide research carried out by him in the Laboratory of Nanoscience and Technology (LNT), Department of Physics under my supervision. I believe that this thesis fulfills part of the requirement for the award of Master of Philosophy. The result embodied in the thesis has not been submitted for the award of any other degree.

Chairman
Dr. Kashif Sabeeh
Department of Physics
Quaid-i-Azam University
Islamabad, Pakistan

Supervisor
Prof. Javed Iqbal Saggu
Department of Physics
Quaid-i-Azam University
Islamabad, Pakistan

Dedicated

To

My Parents

&

Siblings

Declaration

I, Muhammad Oneeb, hereby declare that the project "**Study of V_2O_5-GNPs Nanocomposites as a Promising Electrode Material for Supercapacitors Applications"** submitted by me under the guidance and supervision of Prof. Javed Iqbal Saggu, Professor at Quaid-i-Azam university Islamabad is my work and has not been submitted to any other university, institute or published earlier. The plagiarism test has been carried out using Turnitin software and lies in the permissible range. However, at any stage, if this work is found to be plagiarized, I (Muhammad Oneeb) will be held responsible for it as per rules and regulations.

Muhammad Oneeb

ACKNOWLEDGMENT

First and foremost, praises and thanks to **Allah (SWT)**, for His showers of blessings throughout my research work to complete this dissertation successfully. Thousands of blessings upon **Prophet Muhammad (S.A.W.W)** who is indeed an ideal source of guidance for the entire humanity.

I would like to express my special thanks of gratitude to my teachers, especially my supervisor **Prof. Javed Iqbal Saggu**, who gave me the great opportunity to do this wonderful project. Besides, his motivation, support, and persistent encouragement made me reach my destiny. He was always inspirational in my research work.

I will also pay special thanks to my laboratory mates who were always cooperative in my work. Their guidance and support were important throughout my research work. I will mention especially Ms. Asifa Mumtaz, Mr. Qudrat Ullah, Ms. Amara, Ms. Rida, Ms. Saba ibrar, Mr. Ahmad Hassan Khan, Mr. Ameen, and Mr. Muhammad Usama Jansher. They helped me in the completion of my work within the limited time frame. I would like to thank them for their friendship, empathy, and enthusiastic sense of humor. I am also thankful to all other fellows Abid Khattak, Muhammad Noman, Mazz, and Muhammad Waqas, they gave me valuable ideas, encouragement, better discussion, and a lot of good concepts.

Especially, thanks to my grandfather Mr. Zar Pio Khan, and my uncles who were part of this journey. Indeed, it was the prayers of my beloved Mother and dear father. Finally, it was the tiresome efforts of my Sister Ms. Saira, my beloved Cousin Mr. Imran Khan, my roommate Mr. Amir Iqbal, and Mr. Muhammad Osama who made it possible for me by keeping away every possible difficulty.

Table of Contents

List of Figures

List of Tables

Abstract

Energy storage is an essential for the growth of renewable energy sources, the decentralization of energy production, and demand control due to the erratic nature of energy sources. Supercapacitors and batteries are considered to be the most effective energy storage devices. Recently, research has focused on vanadium pentoxide because of its outstanding electrochemical potential in supercapacitors as electrode material. By lowering the rate of V_2O_5 agglomeration, its composition has been made with GNPs to improve conductivity, electrode porosity, and electrode surface area. V_2O_5 NPs have been fabricated using a simple and flexible Sol-gel method, whereas V_2O_5/GNPs nanocomposites have been synthesized using an ex-situ approach. The structural analysis has been carried out using X-ray diffraction, and FTIR spectroscopy. Different ratios of the GNPs in the V_2O_5 matrix have tuned its bandgap towards visible range. The electrochemical properties of pristine V_2O_5, GNPs, and its V_2O_5-Graphene (GNPs) nanocomposites are examined through different electrochemical technique namely, cyclic voltammetry (CV), Galvano-static charge-discharge (GCD), and electrochemical impedance spectroscopy (EIS), the electrochemical properties of. In particular, the nanocomposites $(V_2O_5)_{0.50}$ $(GNPs)_{0.50}$ maintained 96.3% of the initial capacitance even at 10 Ag^{-1} current density and has a high specific capacitance of 800 Fg^{-1} at a current density of 2 Ag^{-1} from Galvanostatic Charge Discharge (GCD), 1193 Fg^{-1} at a 5mV/s from cyclic voltammetry is obtained. The calculated Ohmic resistance is about 0.44 Ω in a medium of 2M NaOH electrolyte. Supercapacitors made of $(V_2O_5)_{0.50}(GNPs)_{0.50}$ electrode materials have higher energy densities of 27.3 WhKg-1 at a power density of 900 WKg-1 in comparison to the majority of previously reported supercapacitors.

Chapter No. 1 Introduction

1.1 Material Science

The production of physical goods has been closely tied to innovation and the growth of cultures. Earlier civilizations were categorized based on their material growth, with the Stone Age, Bronze Age, and Iron Age comprising the three-age system. Materials continue to be a critical aspect of modern society, influencing every aspect of daily life. To keep up with the demands of modern civilization, the technology requires development of new materials with enhanced properties [1].

Materials have been divided into three primary categories based on atomic bonding including metals, ceramics, and polymers. Modern electronic industry with high-tech applications requires complicated and sophisticated devices, which in turn demand advanced materials. Semiconductors, biomaterials, and futuristic materials are all examples of advanced materials. The learning of interactions between the structure, and properties of materials and their applications is referred to material science. The fundamental arrangement of atoms and molecules at the submicroscopic level is the basis of material structure.

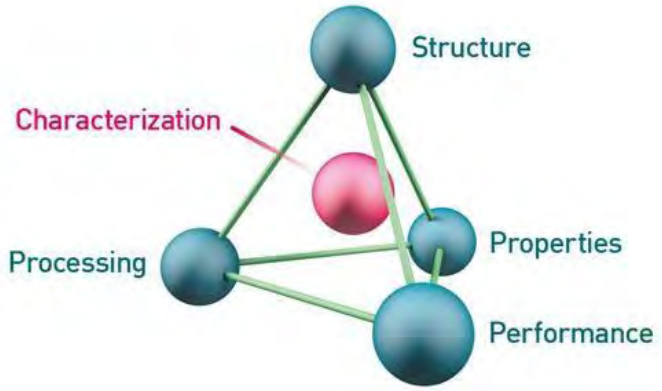

Figure 1.1: Interrelated components of Material Science [2]

As illustrated in Figure 1.1, the discipline of Material Science is primarily composed of four important components: processing, structure, characteristics, and performance. While a material's final performance is a result of its qualities and its material's structure depends on how it has been processed. To choose the optimal material with the attributes necessary for particular applications, one must be aware of how properties, processing, and structure are related. The

stepwise technical development is also a result of the expansion of the variety of suitable material types.

1.2 Introduction to Nanoscience and Nanotechnology

The Greek term "Nanos" implies "Dwarf," or something that requires a magnifying lens to view because it is so little. Nanoparticles are particles that have dimensions of the 10^{-9}m scale, typically ranging from 1 to 100 nanometers (nm). The Understanding of sizes, shapes, and characteristics of materials at the nanoscale is the focus of nanoscience. It seeks to efficiently develop nanoscale structures and gadgets for use in daily life. Nanotechnology is the use of nanostructure in various technology. It involves the creation, design, and application of materials. It also includes gadgets with nanoscale size and shape. At the nanoscale, distinct physical, electrical, chemical, and mechanical properties can be observed. The Nanotechnology finds applications in subjects like Physics, Biology, Chemistry, Engineering, and Material Science.

1.2.1 History

There is a long history of nanotechnology and nanoscience. According to Michael Faraday, the optical characteristics of gold in bulk and gold at nanoscale are very dissimilar. Richard Feynman introduced the concept of nanotechnologies in a presentation titled “There is Plenty of Room at the Bottom" in 1959. Dr. N. Taniguchi, a professor at Tokyo Science University, first used the phrase in the scientific community in 1947. The father of nanotechnology is Kim Eric Dexler, who wrote the first book on the subject, "Engines of Creation and Coming Age of Technology.

The Lycurgus cup, which is composed of dichroic glass and exhibits many types when illuminated, is an example of how Greeks employed it without giving it a name. Nearly 70 nm-sized silver and gold nanoparticles made up the glass. The cup's internally opaque green tint transforms into a gleaming translucent red when exposed to light [3]. The ratios of nanoparticles ware mixed by architect without being aware of the technology. They were only aware of how to combine nanoparticles of various sizes and ratios to create stunning images. Homes and churches were decorated with these nanoparticle materials.

1.3 Energy Storage

Due to limited natural resources and the growing population, the issues with energy generation and storage are now at the forefront of the list of problems that need to be resolved

(e.g., fossil fuels, etc.). Humans cannot solely rely on renewable energy sources in the modern days, or at least not for the foreseeable future. Theoretical estimates of an ideal scenario show that 100% of the world's energy consumption should be met by renewable energy sources, but this is not achievable. The proportion of renewable energy sources can, however, be raised at the expense of cutting-edge study and its application. The figure 1.2 shows the share of renewable energy compared to other energy sources according to the 2021 report.

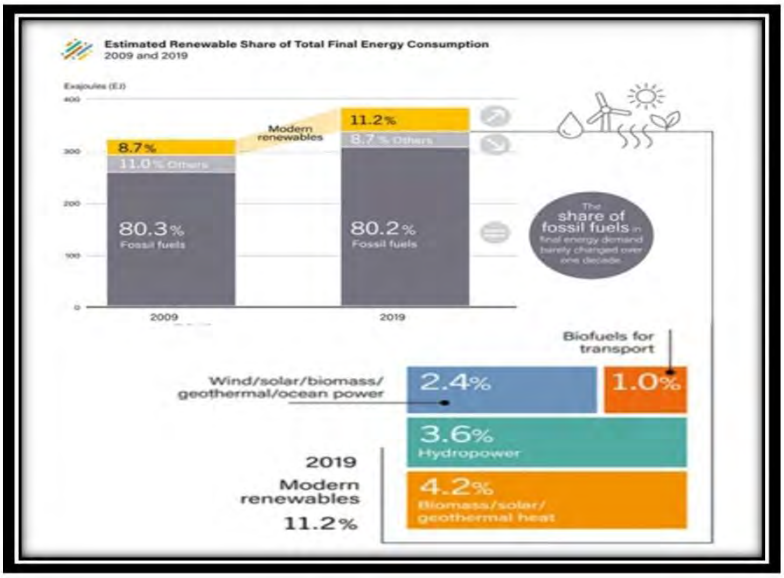

Figure 1.2: The Renewable energy share among other types of energy sources 2021 report [4]

1.3.1 Batteries

Batteries are frequently employed as Energy storage devices (ESDs). Batteries stand out among the well-known ESDs due to unique characteristics such as cyclic charge-discharge, portability, ease of use, and a wide range of power storage (100 W to 20 MW) [5]. The activation of chemical reactions within each battery cell, followed by the conversion of chemical energy into electrical energy, makes up the charging and discharging mechanism of batteries. Lithium-Ion Batteries (LIBs), Lead Acid Batteries (LAB), Nickel-Zinc Batteries (NIB), Sodium-Ion Batteries (SIB), and nickel-cadmium batteries are among the several types of batteries utilized (NiCd). Due to their low self-discharge rate, the capacity for operation at high voltages, and high energy densities in comparison to other battery choices, Ni-Cd and LIB batteries are among the most popular [6].

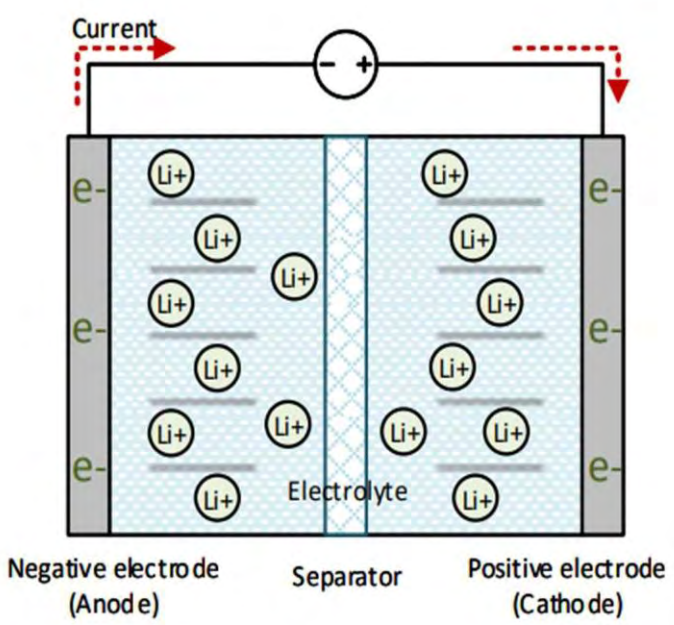

Figure 1.3: A schematic diagram of Li-Ion Battery's charge-discharge mechanism [7]

Li^+ ions transport serves as the foundation for LIBs' primary charge-discharge mechanism as shown in the figure 1.3. While the discharge of LIBs is provided by the opposite transfer of Li-ions, the transfer of Li^+ ions through the electrolyte from the cathode toward the anode electrode and separator supports its charge accumulation process. Equation (1.1) illustrates the LIBs' redox process:

$$LiMO_2 + C_6 \longleftrightarrow LixC_6 + Li_{(1-x)}(MO_2)_x \quad (1.1)$$

1.3.2 Capacitors

The equipment used to store the electrical charge is called a capacitor. Electrostatic and electrolytic capacitors are the two main types of these. The low capacitance of electrostatic capacitors, which ranges from a few Pico Farads (pF) to a few Micro Farads, allows them to store electrostatic energy quickly. On the other hand, the capacitance of electrolytic capacitors for storing electrical energy is larger. There are numerous applications such as filtering, buffering, and electrostatic transducers, make use of these capacitors. Through dielectric material, the parallel plates in conventional capacitors are separated. Charge transfer takes place when electrode plates of the device are subjected to a potential difference (P.D), causing the accumulation of charge on the plates until they reach a state of equilibrium characterized by the

desired potential difference between them. The following equation (1.2) is used to compute the capacitance of parallel plate capacitors.

$$\boldsymbol{C} = \epsilon_0 \frac{A}{d} \qquad (1.2)$$

Where "$\boldsymbol{\epsilon_0}$" denotes the free space permittivity, "A" represents surface area of the plate, and "d" denotes the separation between the plates. The capacitance C is the ratio of the amount of charge "q" on either conductor to the potential difference "V" between the conductors as shown in equation 1.3.

$$\mathbf{C} = \frac{\mathbf{Q}}{\mathbf{V}} \qquad (1.2)$$

where "C" represents capacitance of the capacitor, "Q" is for the net stored charge on the plates, and "V" is for the applied potential. The capacitance and potential put across a capacitor's plates determine how much energy it can store. The relation that can be used to determine the power and energy densities of conventional capacitors is as follows:

$$\boldsymbol{E} = \frac{CV^2}{2} \qquad (1.4)$$

$$P = IV = \frac{V^2}{4} \qquad (1.5)$$

Where "P" and "E" are the power and energy densities respectively, and "I","V", and "R" represents current through the system, applied potential and resistance respectively.

1.3.3 Supercapacitors

Supercapacitors are considered as emerging candidate for high-performance devices, with the potential to enable a wide range of applications in advanced technologies. The true significance of supercapacitors becomes apparent when their energy and power densities are optimized. The primary areas of research emphasis lie in developing electrode materials, refining fabrication techniques, and fine-tuning the electrolyte and electrode materials to achieve the necessary attributes and performance of these supercapacitors. Electrochemical and ultracapacitors are other names for supercapacitors. A supercapacitor consists of two electrodes with high surface area and incredibly thin dielectric layer. Carbonaceous materials are often used to enhance surface area of the plates because of their porous nature. Thus, in comparison to conventional capacitors, these supercapacitors have a specific capacitance that is many orders of magnitude higher [8]. Supercapacitors are used in a variety of applications for energy storage, either alone or in combination with fuel cells and batteries. Supercapacitors are more promising

than conventional energy storage devices due to their high-power potential, many charge-discharge cycles, and stable thermal operating range. Compared to rechargeable batteries, supercapacitors can store more energy and have a greater power supply rate. Supercapacitors can't compete with the energy density of fuel cells and batteries. This demands integration with fuel cells and batteries and other sources like power, for applications that require an energy source for a considerable amount of time [9]. As a result, the researcher's new goal is to enhance SC's energy density in comparison to batteries. Both supercapacitors and ultracapacitors are used to store energy in form of electrical energy are similar to regular capacitors but differ in two key respects. Its plates possess a large area as compared to an ordinary capacitor. As a result of the separator utilized in SCs functioning differently than a standard dielectric, there is very little separation between the plates. In contrast to an ordinary capacitor, which uses a solid or dry substance as a dielectric medium, a supercapacitor's electrodes are separated by a liquid or wet electrolyte.

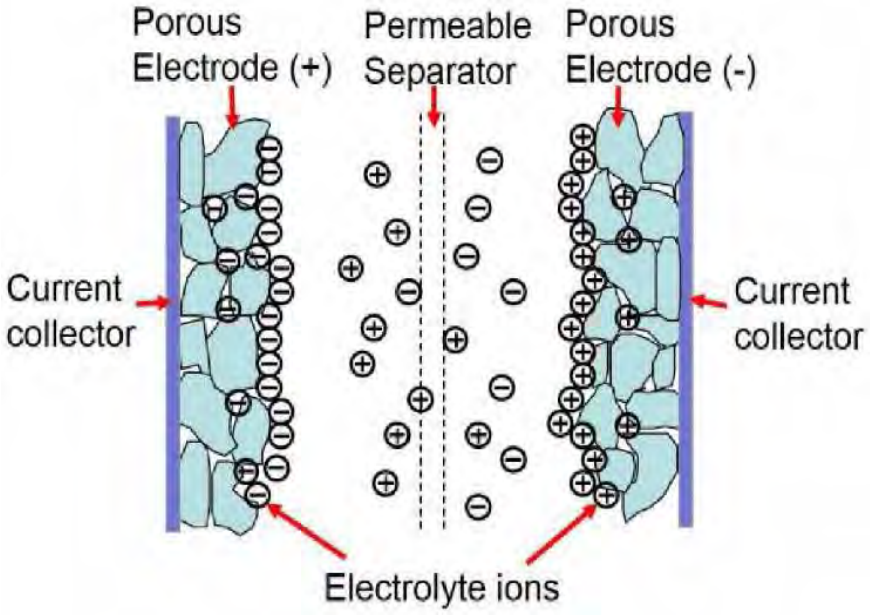

Figure 1.4: A schematic diagram of a supercapacitor construction [10]

A supercapacitor is made up of two metallic plates (electrodes) that are connected ionically and are spaced apart by a separator and an "electrolyte" (a material dissolved in water). The porous material, typically carbonaceous materials, is deposited on the metallic electrodes which consequently increases the electrode surface area for applications involving charge

storage. Since they are porous, plates act like electrical absorbing sponges. A schematic diagram for a supercapacitor construction is depicted by the Figure 1.3.

Potential difference applied across its end, polarizes the ions in electrolytes which separate and create double layer in electrode surface about one ion size. Both electrodes have a balanced charge layer and an interface with an opposing ionic charge layer. The ions from the double layer are likely to be absorbed by the surface area of the electrode, resulting in the pseudocapacitive phenomena. Frequently, the kind of surface area of electrode materials encourages this phenomenon. The basic formula for conventional capacitors, which are given in equation 1.6 is used the capacitance of supercapacitors (1.6).

$$\boldsymbol{C = \epsilon_0 \epsilon_r \frac{A}{d}} \qquad (1.6)$$

Where "A" stands for "surface area" of the electrodes, " ϵ_0" stand for "relative permittivity of the dielectric material, and "ϵ_r" are, represents "permittivity of free space," respectively. "d" stands for “distance between two electrodes” with opposing charges.

1.3.4 Conventional Capacitors and Electrochemical Supercapacitors

An energy-storing component called a conventional capacitor often referred to as an electrostatic capacitor or condenser, is made up of two electrically conductive plates (electrodes) having a dielectric layer between them. Insulators including ceramic, glass, paper, plastic, and aluminum oxide are used as dielectric materials (Al_2O_3). The Capacitor charging is an easy operation. When two conductive plates are connected to an external power source, negative charges accumulate on one plate while positive charges accumulate on the other, resulting in a potential difference between the two plates. When a capacitor keeps charges on each of its individual plates even after the external power source has been disconnected, it is said to be in a charged condition. Upon discharge, the capacitor releases its stored energy to a connected resistive load by exchanging its positive and negative charges. However, the low energy capacity of these common capacitors limits their application. As a result of the search for a novel alternative material, a new class of capacitors called supercapacitors or ECs was developed. In contrast to conventional capacitors, electrostatic separation (ES) electrodes are typically made of very porous materials, like carbon and the separator is either liquid or solid, leading to the generation of electrode-electrolyte interfaces These interfaces are known as electric double layers that can store more charges because they have a greater surface area than dielectric

capacitors. It is acknowledged that an ES's unique structure enables greater energy storage than is possible with ordinary capacitors. A section is offered to address the extensive examination of ES's foundational concepts. It would be helpful to quickly review the development of this energy storage technology before going into the ES fundamentals.

1.4 Electrochemical Supercapacitors Importance

Electrochemical supercapacitors (ESs) provide benefits that make up for the various shortcomings of other viable energy storage devices, which has sparked a lot of research and commercial interest Compared to fuel cells and batteries, compared to conventional capacitors, ESs can produce higher power and energy densities. A Ragone plot comparing the specific power and specific energy of well-known energy storage and conversion systems as shown in Figure 1.5. The supercapacitor technology may bridge the energy and power density gap between capacitors and batteries, as shown in Figure 1.5. Additionally, supercapacitors outlast batteries in terms of cycle life because they undergo significantly fewer chemical phase transitions during continuous charging and discharging than batteries. The Supercapacitors are more adaptable as high-powered energy storage because of these crucial characteristics. Batteries and supercapacitors have been highlighted by the Department of Energy in the US (DOE) as important future energy storage technologies [11].

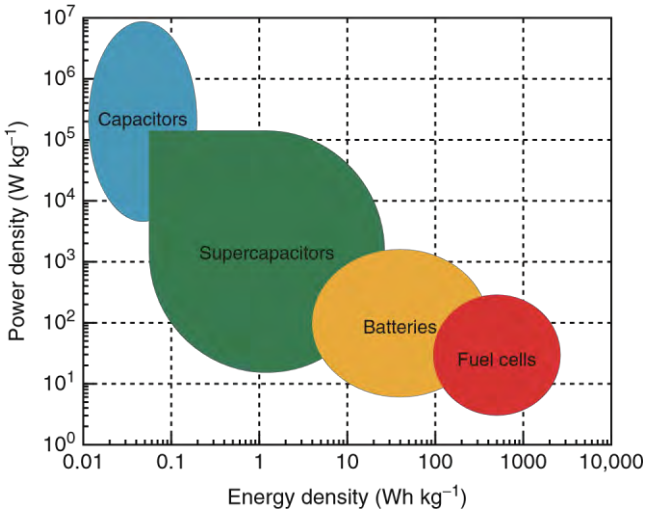

Figure 1.5: Ragone plot for significant energy storage and conversion devices [12]

The first use of ESs was as an electronic backup power source. Supercapacitors are perfect for providing rapid and uninterrupted backup power in reaction to energy surges since they can discharge huge power in a few seconds. However, batteries are less than ideal for this

kind of application due to their higher cost and potential for unpredictable temperature increases. Supercapacitors can be used in both consumer and military systems. Supercapacitor-powered portable cordless screwdrivers made by Coleman are currently available for home use. This power tool has a 90 percent charge and is ready to use right away [13]. Supercapacitors are typically installed and used in military applications as an alternate power source for helicopters, black boxes, and so many others.

The energy recovery in hybrid electric vehicles (HEV) and public transportation has further rekindled interest in supercapacitors. Supercapacitors may store the immediate energy from the brakes and discharge to when needed, increase the fuel economy. Furthermore, the present HEVs struggle with temperature stability issues because of the unwanted heat that resistances and exothermic reactions produce throughout the charging and discharging processes. Supercapacitors can be used in HEVs to handle thermal difficulties because they have the capacity to disperse heat effectively. This makes it easier for them to enter the HEV market.

1.5 Types of Supercapacitors

ES (Electrostatic) capacitors were developed by researchers during the mid-1900s. These capacitors have the unique ability to store exceptionally high amounts of charge. This is made possible by the presence of charges in the form of electric double layer located at the interfaces between the electrodes and the electrolyte. The advancement of ES (Electrostatic) technology, driven by the rapid growth of mobile devices and hybrid cars, led to the development of pseudocapacitors and asymmetric supercapacitors. These two types of ESs emerged alongside electrostatic double-layer supercapacitors. In the subsequent sections, we will research into the characteristics of these three ES variants, as well as explore the energy storage mechanisms employed by conventional capacitors.

1.5.1 Electrostatic Double Layer Capacitor (EDLCs)

The mechanism of EDLCs and conventional Capacitors is similar. However, as opposed to charges kept in the dielectric layer, EDLCs store their energy at the interfaces between the electrode and the electrolyte. A voltage differential across the electrochemical double-layer capacitors (EDLCs) as shown in figure 1.6 causes electrolyte ions to migrate to the micropores of the electrode materials, resulting in the formation of electrodes with contrasting polarities. In contrast to conventional capacitors, the separator's thickness controls the capacitance. The double layer thickness of the electrode/electrolyte interface controls the capacitance of EDLC

(Figure 1.6). The double layer thickness is significantly less than the separator, a typical capacitor has a significantly smaller capacitance than a EDLCs [14]. In addition to having a smaller separation distance, an EDLC's capacitance can be improved by having an electrode/electrolyte interface with a substantially higher surface area than in conventional capacitors. Additionally, the strong electrical conductivity of the electrolyte in the EDLC can lower the electrode's internal resistance.

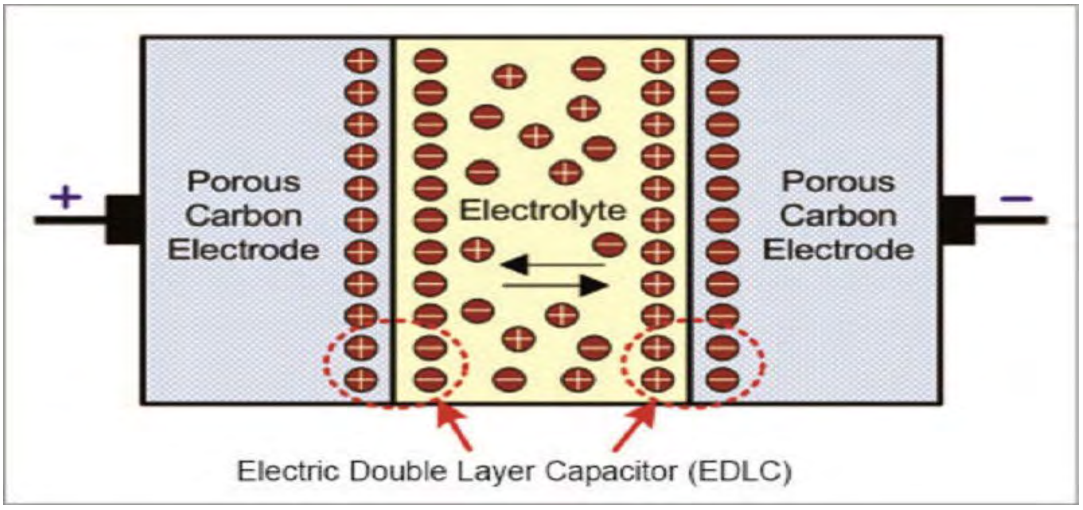

Figure 1.6: A schematic of charged EDLCs [15]

The commercial EDLCs often make extensive use of activated carbon (AC), a particular kind of abundant and affordable carbon. In organic electrolytes, AC can display specific capacitance of 102–120 Fg^{-1} [16]. Recent developments have created complex carbon structures like organized CNTs, mesoporous carbon, and graphene to additional enhance the capacitance of AC materials. For instance, KOH-activated graphene created exhibits an extreme specific capacitance of 166 Fg^{-1} in organic electrolytes [17].

1.5.2 Pseudocapacitors

Pseudocapacitors, often referred to as electrochemical pseudocapacitors, differ from EDLCs in that they use oxidation-reduction (Redox) reactions, electro sorption, and an intercalation mechanism to store energy [18], Using electrode materials like "metal oxides" and "conducting polymers" [19]. Due to the faradic processes, a pseudocapacitors has larger "Cs" value and "Eg" value than EDLCs. Pseudocapacitors rely on an electronic charge transfer from an ion that has been "de-solvated" and adsorbed to the electrolyte and electrode. Furthermore, no interaction between adsorbed ions and the material atoms in the mechanism, therefore only the

transfer of charge takes place. When an electrode surface absorbs ions, it has a chemical affinity with those ions, which affects whether or not the electrodes will eventually attain pseudo-capacitance capacity as shown in the figure 1.7. For the effect (electrode), the structure and dimensional shape of the pores is also crucial. With this applied voltage, charge storage in pseudocapacitors rises linearly. Pseudocapactors utilize conducting polymers including polyphenylene vinylene (PPV), polyaniline (PANI), polypyrrole (PPY), polythiophene, and polyacetylene, as well as transition-metal oxides (TMO) as CO_3O_4, NiO, MnO_2, V_2O_5, Iron oxide, RuO_2, and transition metal sulphides.

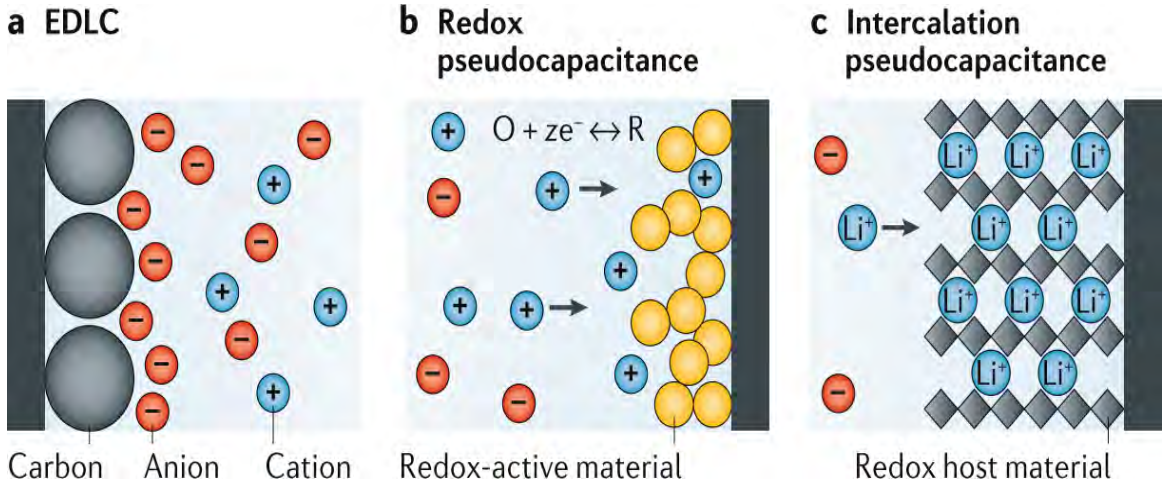

Figure 1.7: A schematic diagram of pseudocapacitors [20]

1.5.3 Hybrid Capacitors

As the name implies, hybrid capacitors must possess both the characteristics of an EDLC and a pseudocapacitor. Their components use electrodes with a variety of characteristics, including an electrode with electrostatic capacitance and an electrode with electrochemical capacitance. This particular supercapacitor has asymmetric electrodes, primarily displaying electrostatic capacitance and other electrochemical capacitance. Additionally, hitherto unachievable performance features were merged into the hybrid capacitors. Additionally, they are integrating the best aspects of SCs and EDLCs into a single unit. Hybrid capacitors were less explored than pseudo-capacitors or EDLCs, but there were ongoing efforts to make them better and to create hybrid capacitors. Due to the immense simplicity with which hybrid capacitors can be designed and tuned, as well as the increased emphasis on creating SCs with high energy and long cycle lives, hybrid capacitors have eclipsed EDLCs as the dominant SC class. These three

groups differentiated on the basis of electrode configuration were divided into three types such as battery-type capacitors, asymmetric, and composite type.

1.5.3.1 Composite

The use of metal oxides or carbon-based materials having polymer conduction in a single electrode by composite electrodes suggests that the electrode will have both chemical and physical processes for storing energy. The Composites come in two varieties i.e., binary composites, which are electrodes comprised of only two components, and ternary composites, which are electrodes built of three different materials [21].

1.5.3.2 Asymmetric

Hybrid capacitors combines non-faradic and faradic processes with an EDLC and a pseudo capacitor electrode. In this way, the carbon material served as the negative electrode and the metal oxide and conducting polymer as the positive electrode.

1.5.3.3 Battery Type

This innovation presents an exclusive combination of supercapacitors (SCs) and battery electrodes, merging the rapid recharge capability of SCs with the energy storage capacity of batteries within a single cell. This breakthrough addresses the demand for more efficient rechargeable batteries and high-capacity capacitors. Surprisingly, there has been limited research on hybrid systems that integrate both battery and supercapacitor technologies [22].

1.5.4 Asymmetric Supercapacitor

An asymmetric supercapacitor, as its name suggests, is built using electrodes that are different from one another. A capacitive electrode that resembles carbonaceous material with a battery like faradaic electrode. Due to the redox process in electrode materials, this innovative design allows for improvement in energy density [23]. However, both electrodes must be optimized by a careful design. Amatucci et al. (2001) created the first asymmetric supercapacitor prototype, and many different research teams had followed. For instance, Wu et al. (2010) fabricated a supercapacitor-like asymmetric with a highly energy density made of MnO_2 nanowires and graphene [24]. As compared to symmetric supercapacitors made of graphene-graphene nano composites (2.8Wh kg^{-1}) and manganese oxide-manganese oxide (5.2Wh kg^{-1}), the asymmetric manganese oxide-graphene configuration demonstrated a notable advantage in energy density. By incorporating manganese oxide into graphene as an electrode and completing

it with an activated carbon nanofiber-based electrode, the energy density was further increased [25]. Although symmetric supercapacitors have worse energy densities than asymmetric supercapacitors, the use of faradaic materials in the electrodes may be to reduce the retentivity. Despite this, asymmetric supercapacitors have a promising future in SCs and batteries [26].

1.6 Electrolytes

One of the most important elements of electrochemical supercapacitors (ESs) is the electrolyte, which is composed of salt and an electrolyte solvent. It offers a route to ionic conductivity and permits charge adjustment between the cell's electrodes. The formation of the electric double layer (EDL) in EDLC and the reversible redox process involved in charge storage in pseudocapacitors are both significantly influenced by the electrolyte.

The EDLCs and pseudocapacitance capacitance, energy, and power densities, as well as the retentivity of the ESs, are all significantly influenced by the composition of the electrolyte. The potential window, ion concentration, solvent selection, solvent-ion interactions, electrolyte-electrode material interactions, and ion type and size all affect how the ES behaves and performs. As an illustration, the electrochemical stable potential window (V) of the electrolyte determines the operational cell voltage and subsequently influences both power and energy densities. The power density is significantly influenced by the electrolyte's ion conductivity, which is directly related to the ES's ESR. The lifetime and self-discharge of electrochemical supercapacitors may also be impacted by interactions between ions and solvents as well as electrolyte and electrode materials. Liquid electrolytes and solid/quasi solid-state electrolytes are two different forms of electrolytes that have been reported in the literature. Aqueous electrolytes, organic electrolytes, and ionic liquids are further categories for liquid electrolytes, while organic electrolytes and inorganic electrolytes can be roughly categorized as solid or quasi-solid-state electrolytes. Despite the numerous varieties of electrolytes, none have yet satiated all the conditions mentioned above. The classification of electrolytes for electrochemical supercapacitors as shown in the figure 1.8.

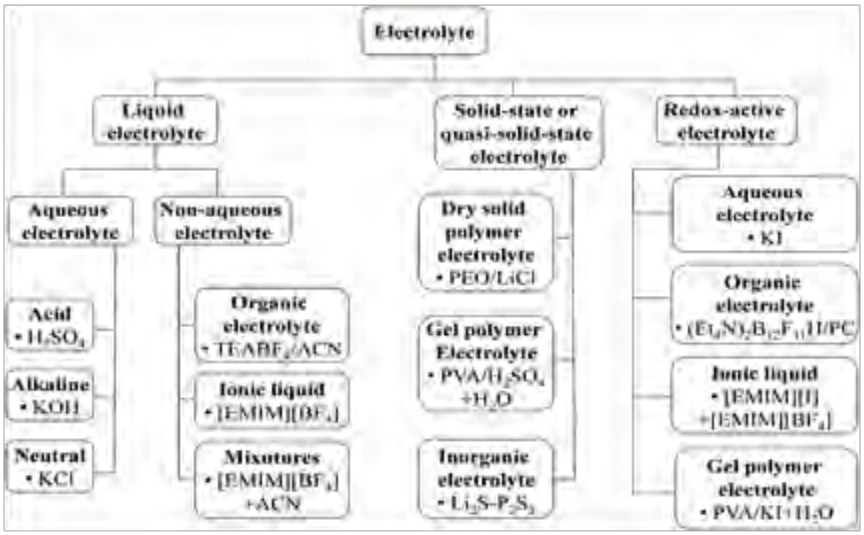

Figure 1.8: Classification of electrolytes for electrochemical supercapacitors

1.6.1 Aqueous Electrolytes

Aqueous electrolytes, although typically is used in commercial energy storage products because of high energy density, are a desirable option in the laboratory due to their cheap cost and ease of handling. Other electrolytes such as ionic liquids, organic electrolytes, and aqueous electrolytes do not require complicated purification procedures and can be handled under normal conditions. The conductivity of aqueous electrolytes is extremely high and is orders of magnitude greater than that of organic and ionic liquid electrolytes. They can be divided into three categories i.e., acid solutions, alkaline solutions, and neutral solutions. Examples of the former two groups are sulfuric acid, potassium hydroxide, and sodium sulphate [27].

1.6.1.1 Strong Acid Electrolytes

Acidic electrolytes are a popular choice for energy storage studies, with sulfuric acid being the most frequently used among different acidic electrolytes. This is because of its very huge ionic conductivity, which is strongly dependent on its concentration. According to studies, the sulfuric acid electrolyte reaches its maximum ionic conductivity at 1.0 M concentration at 25°C. As a result, the mainstream of energy storage studies using carbon-based electrode materials utilize a 1.0 M sulfuric acid electrolyte solution. The sulfuric acid has maximum ionic conductivity up to 0.8 S/cm for a 1 Mole solution.

1.6.1.2 Strong Acid Electrolytes for EDLCs

The majority of comparative research in the literature demonstrates that EDLCs in sulfuric acid (H_2SO_4) electrolytes have larger specific capacitances than those in neutral electrolytes. Additionally, due to sulfuric acid's stronger ionic conductivity, the equivalent series resistance (ESR) of energy storage devices using neutral electrolytes is often larger than that of sulfuric acid. According to studies, there is a correlation between the conductivity of the electrolyte and the specific capacitance of activated carbons. As conductivity increases, so does specific capacitance, and the electrode material contributes more than the electrolyte does. This is due to the close relationship between ion mobility and electrolyte conductivity. In recent years, studies have mainly reported specific capacitances of EDLC with acidic electrolytes such as the sulfuric acid to be in the measure of 100 to 298 F/g, which is almost higher than organic electrolytes [28-29], Carbon-based electrode materials are the major contributor to the specific capacitance, with the electrolyte contribution being less significant. This has been confirmed in many reviews [30].

1.6.1.3 Strong Acid Electrolytes for Pseudocapacitors

Research have been done to enhance the energy density of EDLCs by investigating other types of energy storage systems, like pseudocapacitors. It was discovered that carbon-based electrode materials, when used H_2SO_4 electrolytes, showed pseudocapacitive properties in addition to their electrostatic EDL capacitance [31]. This is because the surface functionalities of the material, like oxygenated carbon, undergo fast redox reactions. For example, when used in acidic aqueous electrolytes like H_2SO_4, pseudocapacitive effects are produced due to surface modification because of the involvement of protons in the redox processes. However, this effect is not observed in alkaline electrolytes [32]. However, due to the deterioration of the electrode functional materials in aqueous electrolytes, the lifespan of EDLCs is often greater than that of pseudocapacitors. However, compared to aqueous electrolytes, the cycle lifetimes of ESs are substantially longer when utilized with organic electrolytes. It results from organic electrolytes capacitance, which is mostly caused by electrostatic charge separation [33].

1.6.1.4 Strong Acidic Electrolytes for Hybrid Capacitors

Enhancing the energy densities of aqueous electrolyte-based energy storage systems (ESs) is the goal of the development of hybrid supercapacitors. The highest voltage that may be produced in symmetric electrochemical cells with the identical electrode materials in aqueous

electrolytes, such as H_2SO_4 or KOH, is restricted due to the occurrence of gas evolution reactions [34]. If an ECs has an asymmetric configuration with different electrode materials, it can have a wider potential voltage even in aqueous electrolytes. This is because in separate potential windows, different electrodes can work complementarily. An electrochemical system can have a voltage window that is larger than the thermodynamic range of water, for example, if the positive electrode is carbon-based and has a high potential for the evolution of H_2 and the negative electrode is battery-like or pseudocapacitive and has a high potential for the evolution of O_2. Several asymmetric ESs have been successfully tested in strong acid electrolytes, suggesting their potential for use in real-world applications. These include carbon-lead dioxide, carbon-ruthenium oxide, carbon-ECPs, and carbon with distinct characteristics in each electrode [35].

1.6.2 Alkaline Electrolytes

1.6.2.1 Alkaline Electrolytes for EDLC

Alkaline electrolytes improve energy storage in electrochemical capacitors. It has been tried to use base electrolytes, such as aqueous KOH, instead of strong acid electrolytes to improve energy storage in electrochemical capacitors (ESs). Several methods have been used to increase the energy density of ESs:

1. Improving the capacitance of carbon-based electrodes through the incorporation of a pseudocapacitive component.
2. Combining carbon-based materials and pseudocapacitive materials to form composite materials.
3. Expanding the voltage range of base electrolytes by utilizing asymmetric electrochemical systems (ESs) in their design.

1.6.2.2 Alkaline Electrolytes for Pseudocapacitors

The interaction among ions present in the electrolyte and functional groups on the surface of the carbon plays a role in the link between the pseudo capacitance of graphene-based electrode materials and faradaic interactions [36]. Electrolytes can be used to increase the efficiency of nitrogen (N)-doped carbon electrode materials, according to research. This result implies that the pH value and the particular kind of electrolyte used have a substantial impact on pseudo capacitance [37]. Additionally, it has been demonstrated that co-doping carbon with nitrogen and phosphorus yields higher specific capacitance, better stability, and a larger potential window compared to materials without phosphorus, improving ES performance [38-39]. The performance

of ESs is affected by various factors, involving the type of ion, concentration, and operating temperature of the electrolyte. The electrolyte concentration, for instance, has been shown to impact the equivalent series resistance (ESR) value, [40] specific capacitance, and Oxygen evolution reaction [41]. Applying a concentrated electrolyte solution could cause corrosion on the electrode substrate's surface, which might eventually cause the electrode material to separate from the substrate. Therefore, it is crucial to optimize the electrolyte content in order to enhance the ES's overall performance. Due to enhanced ion diffusion in the electrolyte, a rise in electrolyte temperature frequently causes an increase in specific capacitance and a decrease in ESR. The onset potential necessary for oxygen evolution is reduced as a result of the temperature increase, which speeds up the oxygen evolution reaction at the positive electrode [42-43].

1.6.2.3 Alkaline Electrolytes for Hybrid Capacitors

In present era, the significant scientific efforts have been made to improving the energy density of asymmetric electrochemical supercapacitors (ESs). Alkaline electrolytes have been used as a medium to achieve this goal. The design of asymmetric ESs is unique in the sense that the electrodes are made of different materials. This design helps in achieving a wide potential window that is essential for improving energy density.

The positive electrode of an asymmetric ES can either be a battery-type material, such as medical hydroxide, [44] or a pseudocapacitive material, like ruthenium oxide [45]. In either case, Faradaic reactions are used to store the charge. The negative electrode, on the other hand, is constructed of a material with a carbon base and primarily utilizes the electric double-layer (EDL) effect to store charge. In contrast to the pseudocapacitive positive electrode, which stores charge through both ion transfer and faradaic processes, a battery-type positive electrode in an asymmetric ES enables the storage of charge through the transfer of ions. On the other hand, the carbon-based negative electrode primarily utilizes the EDLC effect to store charge [46]. ESs with asymmetrical electrodes have slower charging/discharging and lower response time compared to EDLCs [47].

1.6.3 Neutral Electrolytes

Similar to alkaline electrolytes, neutral electrolytes have concerned interest in the field of electrochemical storage systems (ESs). These neutral electrolytes have several advantages over their acidic and alkaline close siblings, including a larger operating potential window, low corrosion, and better protection. Some of the often-utilized conducting salts in neutral

electrolytes are Li (such as LiCl and $LiClO_4$), Na (such as NaCl and Na_2SO_4), K (such as KCl and K_2SO_4), Ca (such as $Ca(NO_3)_2$), and Mg (such as $MgSO_4$) salts. The most popular of these neutral electrolytes, Na_2SO_4, has been given to be an electrolyte that has promise for a range of pseudocapacitive materials, especially those based on MnO_2. Although most studies have also concentrated on electrochemical double-layer systems, most pseudocapacitors, and hybrid electrochemical storage systems employ neutral electrolytes. These neutral electrolytes have been extensively studied and have been shown to possess a number of desirable characteristics, including a wider working potential window, lower corrosion rates, and improved safety. In addition to these advantages, neutral electrolytes are also compatible with a wider range of materials, which makes them a versatile option for electrochemical storage systems.

1.6.3.1 Neutral Electrolytes for EDLCs

Studies comparing the performance EDLCs using different electrolytes have shown that those using neutral electrolytes have much lower specific capacitances as compared to those using acidic (H_2SO_4) or alkaline (KOH) electrolytes [48-49] This is because of lower ionic conductivity, resulting in lower equivalent series resistance (ESR). Despite this, carbon based EDLCs with neutral electrolytes have the advantage of wider operating voltage, and stable potential windows (ESPW) of electrolytes are increased when compared to those using acidic or alkaline aqueous electrolytes. The reason for this is that acidic and basic like NaOH electrolytes have a higher abundance of H^+ and OH^- ions compared to neutral electrolytes [50-51].

1.6.3.2 Neutral Electrolytes for Pseudocapacitors

In electrochemical storage devices, Manganese Oxide and Vanadium Pentoxide-based materials have been given to be effective pseudocapacitive materials in neutral electrolytes like Na_2SO_4. Manganese Oxide is the most widely researched material in this area. Numerous variables, including pH, the types of cations and anions present, salt concentrations, additives, and solution temperatures, can affect how well these materials operate [52]. The performance of these materials may also be impacted by the particular cation species. However, it is still unclear how exactly the cation species and particular capacitance relate to one another. Some studies have shown that the use of Li_2SO_4 results in the highest specific capacitance, followed by Na_2SO_4 and then K_2SO_4, which may be related to the order of ionic sizes ($Li^+ > Na^+ > K^+$) [53-54].

1.6.3.3 Neutral Electrolytes for Hybrid Capacitors

Recently symmetric electrochemical capacitors (ESs) have attracted a lot of attention recently, particularly neutral electrolytes. Neutral electrolytes have a lot of attention due to their potential to increase the operating voltage and, consequently, the energy density of asymmetric electrochemical capacitors (ESs). Despite having substantial specific capacitances, some pseudocapacitive materials, such MnO_2, have restricted potential windows that limit the cell voltage and energy density. For symmetrical ESs built on MnO_2, the cell voltage is often close to 1V. However, by extending the cell voltage to a more negative voltage, activated carbons and other alternative electrode materials with complementary potential windows can be used to greatly enhance the voltage of the cell. Although much progress has been made in this area, further improvement is still required to raise the energy density and cycle life of ESs [55]. In summary, neutral electrolytes offer a promising solution to improve the performance of ESs. By replacing the negative electrode with complementary materials and using neutral aqueous electrolytes, the operational voltage and energy density can be increased while addressing corrosion concerns and promoting environmental sustainability.

1.6.4 Organic Electrolytes

Supercapacitors that are readily available for commercial use typically use organic electrolytes. This is due to their wide operating voltage windows in a range of 0 to 2.7V, thereby increasing their energy density to meet commercial standards. Among the two, acetonitrile is the preferred option as it has only one-third of the ionic resistivity of PC. However, the use of acetonitrile comes with its own set of challenges, such as its toxicity and flammability, which pose a risk to safety. A major concern of organic electrolytes is the aging or degradation of carbon electrodes. When these electrodes are exposed to organic electrolytes, they undergo decomposition, which clogs up the pores and reduces the capacitive implementation and cyclic stability of the electrodes. This leads to a decrease in the overall efficiency and lifespan of the supercapacitor, making it less reliable for use in various applications [56].

1.6.5 Ionic Liquids (ILs)

Ionic liquids (ILs) are a type of electrolyte that is unique due to their liquid form at room temperature. They are composed of molten salts and lack any solvents, resulting in low melting temperatures. This property, combined with the fact that they are non-toxic and non-flammable, makes them an attractive option for energy storage devices. The voltage window for ILs is also

the largest of all electrolytes, ranging from 0.0 to 3-5V, without any thermal instability. This, in addition to the ability to heat ILs up to 300ºC without vaporization, makes them a desirable option for high-temperature applications [57]. Research has been conducted on the use of ILs in laser-scribed graphene supercapacitors, and the results showed that IL-based devices outperformed both aqueous- and organic-based devices. Despite these promising results, the high cost of ILs remains a challenge for commercial applications [58].

1.7 Components of Supercapacitor

Supercapacitors can work on the basis of two different mechanisms, depending on the type of electrode materials used. One of these mechanisms is the use of EDLCs, which consist primarily of carbonaceous materials. In EDLCs, charges are stored statically in the porous-like structures of the electrodes. When choosing materials for supercapacitor electrodes, there are several key qualifications that must be considered. Firstly, the materials must have a huge surface area and a high degree of porosity in order to maximize the energy storage capacity of the electrodes. Secondly, good surface wettability is important in order to facilitate the ion exchange process between the electrolyte and the electrode surfaces.

In addition, high electrical conductivity is another important characteristic of suitable electrode materials. This helps to minimize energy losses during the energy storage and discharge processes and ensures that the supercapacitor operates at maximum efficiency. Long cycle stability, with a minimum of 105 cycles, is also important in order to ensure that the supercapacitor remains functional over extended periods of time. Another important consideration when choosing electrode materials is the ease with which the morphology of the materials can be manipulated. This helps to optimize the energy storage capacity of the electrodes and to ensure that the supercapacitor operates at maximum efficiency. Finally, thermodynamic stability over a wide operational potential range is also important. This helps to ensure that the materials remain stable under a wide operating condition and that the supercapacitor continues to function effectively even under extreme environmental conditions.

1.7.1 Carbon Nanotubes (CNTs)

Carbon nanotubes (CNTs) exhibit fascinating characteristics in contrast to activated carbon (AC). Unlike activated carbon (AC), which consists of irregular structures, CNTs are a type of engineered carbon with exceptional properties. CNTs are composed of stacked graphitic walls, organized in a nearly one-dimensional cylindrical structure. Single-walled carbon nanotubes

(SWCNTs) and multi-walled carbon nanotubes (MWCNTs) can be used to further categorize these tubes based on their thickness. The long, one-dimensional structure of CNTs provides exceptional mechanical properties. This results in electrical conductivity that is superior to that of AC. CNT arrays that are highly ordered have a large surface area, which provides ample space for electron storage. The specific capacitance of CNTs, which depends on their morphology and also purity, ranges between 15 and 200 F/g. Despite their many advantages, the high cost of production remains a significant obstacle to the widespread use of CNTs in commercial supercapacitors. Currently, carbon is used to produce small amounts of high-purity CNTs in laboratory settings. However, before these techniques can be used to scale up production and purification, they require further research and development [59].

1.7.2 Graphene

Graphene, a renowned carbon allotrope, is a single-layered material composed of carbon atoms in a two-dimensional hexagonal lattice structure. The name “Graphene” is derived from “Graphite” with the suffix “-ene” reflecting the large number of double bonds present in this carbon allotrope. Every carbon atom in a graphene sheet is attached to its three nearest neighbor atoms through strong δ-bonds. This unique structure gives graphene some remarkable properties.

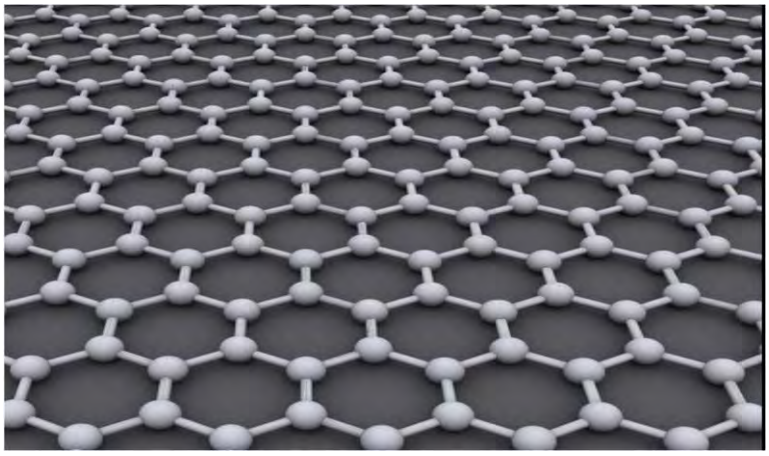

Figure 1.9: Honeycomb hexagonal lattice structure of graphene [60]

Graphene is known to be the thinnest material ever discovered, with a thickness of only one atom, and also one of the strongest. It is a semimetal with good electronic properties, as the

valence band in graphene touches the conduction band. The honeycomb hexagonal lattice structure of graphene as shown in the figure 1.9. The charge carriers in graphene have a high intrinsic mobility and an effective mass of approximately 200,000 $cm^2v^{-1}s^{-1}$. Additionally, graphene has remarkable thermal conductivity, with a value ranging from 4.85 ± 0.45 ×104 to 5.3 ± 0.49 ×109 wm^{-1} k^{-1} [61].

Graphene has high stiffness, with a strength that is 100 to 310 times stronger than steel. Additionally, with a value of 23%, graphene equally absorbs light in the visible and near-infrared spectrums. To sum up, graphene is a distinct carbon allotrope that has drawn a lot of interest because of its extraordinary qualities. Its two-dimensional hexagonal honeycomb lattice structure offers it excellent thermal conductivity, high intrinsic mobility, and strength. It is a semimetal with good electronic characteristics, and because it absorbs light, it can be used in a variety of applications.

1.7.3 Properties of Graphene

The basic properties of Graphene are given in Table (1.1).

Table 1.1: Theoretical properties of Graphene.

Chemical name	Graphene
Appearance	Darkish Grey
Crystal Structure	2D, Hexagonal
Bandgap	Zero – Overlap semi-metal
Surface area	~2600 m^2 g^{-1}
Thermal conductivity	5000 Wm^{-1} K^{-1}
Charge carrier mobility	~250000 cm^2 V^{-1} s^{-1}
Mechanical strength	~1 Tpa
Resistivity	6×10^{-6} Ω cm^{-2}
Density	0.77 mg cm^{-2}
Interacting forces	Van der waal forces
Interatomic distance	1.42 Å
Interlayer distance	3.37 Å

1.7.4 Basic Structure of Graphene

On the periodic table, carbon has an atomic mass of 12 and six protons and electrons. Carbon has the following electrical configuration: $1S^2$, $2S^2$, $2P^2$, with the P orbital having the following three suborbital: P_x, P_y, and P_z. Although these sub-orbitals have equal energy levels, the $2P_z$ orbital is unoccupied, and only the $2P^2$ is occupied by two electrons.

There are three different types of hybridization carbon's valence electrons can go through Sp, sp^2, and sp^3. Three distinct geometries linear, trigonal planar, and tetrahedral are created as a result of these hybridizations. The resulting molecular configurations for these geometries are acetylene, ethyl, and methane. Two orbitals join to create two sp hybrid orbitals that point in opposite directions during the process of sp hybridization, resulting in a linear geometry. This hybridization, for instance, results in the formation of acetylene or ethyne. Three orbitals unite in the sp^2 hybridization to create three sp^2 hybrid orbitals and one unhybridized p orbital. Trigonal planar geometry is the result. One example of a molecule created through sp^2 hybridization is ethylene. Four orbitals join together to create four sp^3 hybrid orbitals during sp^3 hybridization, resulting in a tetrahedral geometry. One example of a molecule created by sp^3 hybridization is methane or CH_4 [62].

1.7.5 Graphene Nanoplatelets (GNPs)

Graphene has extraordinary qualities, a form of carbon, has attracted the interest of scientists and researchers. However, it is difficult and not yet practical for mass production to produce graphene in significant amounts. The scientific world has become very interested in graphene nano-platelets (GNPs) as an alternative because they have features similar to those of graphene but are easier to produce.

GNPs are made up of numerous layers of graphite with thicknesses ranging from 0.7 to 100 nanometers. These layers, which can have up to 10–20 atomic layers, are generated by exfoliating graphite. GNPs are better suited for a variety of applications than graphene oxide because they are easier to manufacture, have a higher aspect ratio, a planar shape, and good electrical and thermal conductivity [63]. GNPs are used for coating and filling applications because of their small weight, which is one of their key advantages. They can be applied neatly as a coating to surfaces, incorporated as a suitable filler to polymers and composites, or utilized alone for certain purposes. Additionally, GNPs are a reliable choice for structural applications because of their good mechanical properties. GNPs have a wide range of uses in a variety of

industries, including electronics, energy, and healthcare, because of their special qualities and inexpensive price. They are employed in the creation of solar cells, batteries, sensors, and conductive inks. GNPs are also utilized in drug delivery systems, where their high aspect ratio and planar shape enhance the therapeutic effectiveness of medicines [64].

1.8 Metal Oxide

As prospective electrode materials for energy storage systems, metal oxide compounds have shown considerable promise. They are preferred because of their availability, environmental friendliness, accessibility, and unique characteristics such a wide range of morphologies and constituents, a sizable surface area, and a high theoretical specific capacitance. These materials have also proven essential in electrochemical supercapacitors' electrodes, where they can boost capacitance by controlling defects and surface/interfaces at the nanoscale. Despite these advantages, metal oxide materials nonetheless encounter substantial challenges that restrict their practical uses. The poor electrical conductivity, erratic volume expansion, and slow ion transport in the bulk phase are some of these difficulties. Therefore, there is a pressing need to investigate functional metal oxide materials with improved electrochemical properties. Researchers are developing new metal oxide materials based on their composition, the development of distinctive nanostructures, electro-conductivity, and oxygen vacancies in order to improve their physical and chemical properties [65].

Advancements in harnessing metal oxides have led to the creation of pseudo-supercapacitors, which enhance energy density at the battery scale while retaining the traditional rapid power discharge of capacitors. This approach effectively bridges the gap between batteries and capacitors, resulting in more efficient energy storage solutions. In order to enhance the surface-specific area and attain outstanding electrochemical characteristics, the design and fabrication of innovative porous nanostructures and composites with carbon materials has become increasingly popular. Researchers can increase the surface area of these composites, which enhances performance by boosting the number of reaction-ready active sites. In conclusion, new opportunities for energy storage have emerged as a result of the discovery of transitional metal oxide materials. As a result of continued research and development, it is becoming clearer how to manage their characteristics and create new materials that can address the problems with metal oxide materials. It is feasible to produce materials with outstanding

electrochemical properties that have the potential to revolutionize the field of energy storage by constructing innovative nanostructures and composites with carbon-based materials [66].

1.8.1 Vanadium Oxide (Vanadia)

Vanadia, also known as vanadium pentoxide, is a solid material with brown-yellow color having chemical formula is V_2O_5. It is a vital component of the industrial world due to use in as industrial catalyst and the main precursor of vanadium alloys. It is an amphoteric oxide and an oxidizing agent despite its high oxidation state. Vanadium pentoxide is a favored option for supercapacitor electrodes due to its ease of manufacture, accessibility, and multilayer porous structure. It is considerably less toxic than the other transition metals Oxides.

Vanadium pentoxide is commonly employed in chemical sensing, electro-chromic and optical switching devices in addition to its uses in supercapacitor electrodes. As an intercalation material in rechargeable batteries with mono/multivalent ions like Li^+, Na^+, and Mg^{2+} ions, among others, it is a versatile material that has found extensive use in a variety of forms and nanocomposites. Vanadium compounds can be lethal in some circumstances, according to recent findings, underscoring the importance of exercising caution while working with them. However, vanadium pentoxide continues to be a very beneficial and adaptable substance with a variety of uses in the industrial, technological, and scientific domains [67].

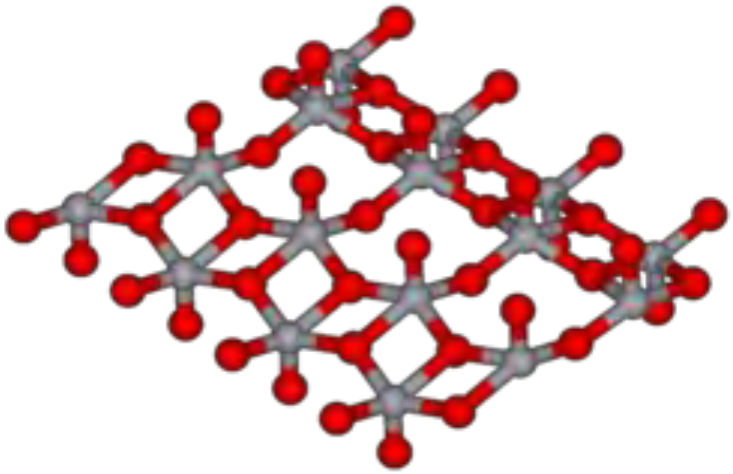

Figure 1.10: Vanadium pentoxide monolayer 3D balls [68]

Amorphous oxides are more isotropic than their anisotropic crystalline counterparts, which leads to less entropic energy loss and faster ionic transport, according to current research. This is due to the fact that homogeneously disordered amorphous materials encourage more percolation routes by creating active diffusion channels than equivalent sized and shaped heterogeneously disordered crystalline materials [69].The structure of Vanadium pentoxide monolayer of 3D balls as shown in the figure 1.10.

In comparison to crystalline forms, the synthesis of amorphous V_2O_5 requires less time, less energy, and costs less money. As a result, using amorphous V_2O_5 has proven to be more advantageous in this regard. Additionally, it has been discovered that hydrated amorphous oxides exhibit increased pseudocapacitive behavior, with a quicker discharge rate even with neutral electrolytes based on large cations. This is due to hydrated oxides with porous morphology having smaller binding energies for chemisorbed electrolyte ions and larger channels for simple ion transit. According to recent studies, even V_2O_5 nanoparticles with rough surfaces have a large specific surface area that significantly boosts electrochemical performance during charging-discharging operations. Finally, amorphous V_2O_5 has many advantages over crystalline versions, such as reduced entropic energy loss, quicker ionic transport, simpler production, and improved electrochemical performance. Due to these benefits, it is a great option, for a supercapacitors and rechargeable batteries energy storage devices as electrode material [70]

Chapter No. 2 Synthesis Techniques

2.1 Introduction

Nanostructures have become an integral part of many advanced applications in different fields like electronics, optics, electrochemistry, environment, and optoelectronics. The synthesis and fabrication of nanostructure and nanocomposites are an essential aspect of nanotechnology. With advances in nanotechnology, there have been numerous techniques introduced to synthesize nanoparticles from various materials like metals, metal oxides, semiconductors, ceramics, metal oxides, and polymers. The origin and synthesis process of the nanoparticles can have an impact on their distinctive morphological, structural, and physicochemical properties. Several methods are available for synthesizing nanoparticles and nanocomposites, including co-precipitation, hydrothermal, sol-gel, inert gas condensation, ion sputtering scattering, microwave, micro-emulsion, solvothermal processing, ball milling, precursor, solid-state, and flame combustion techniques. Every technique has benefits and drawbacks, and the choice of a particular technique depends on the particular demands of the application.

2.1.1 Co-precipitation Method

The way for V_2O_5 nanomaterials to synthesize impacts both their structure and their effectiveness in different applications. There is a different synthesis method for V_2O_5 nanomaterials and how their resulting morphologies affect their electrochemical performance. The co-precipitation synthesis technique is a method used to prepare multicomponent materials. This process involves the formation of intermediate precipitates, often oxalates or hydrous oxides, which result in the creation of a component mixture during precipitation. The aim is to maintain the chemical homogeneity of the final product upon calcination. The co-precipitation synthesis technique involves the preparation of a mixture of aqueous metal salts and a base. The base acts as a precipitating agent which is then collected, washed, and heat-treated for crystallinity. Three mechanisms take place during the co-precipitation synthesis technique: inclusion, adsorption, and occlusion. Inclusion occurs when an impurity atom fills the lattice sites of the host material, causing crystallographic defects. This process of inclusion is conditional and only occurs when the impurity has the same charge and ionic radius as the host material.

Adsorption is another phenomenon that occurs during the co-precipitation synthesis technique. Impurity atoms are loosely bound to the precipitates, forming a weak interaction. This mechanism can contribute to the overall purity of the final product. Occlusion is the third mechanism that occurs during the co-precipitation synthesis technique. This mechanism involves the physical attachment of an adsorbed impurity atom to the precipitates. The impurity atom then grows with the entire crystal. The co-precipitation synthesis technique is a useful method for producing multicomponent materials with high chemical homogeneity. By controlling the factors of the synthesis process, like the temperature and the concentration of the metal salts and base, the properties of the final product can be tailored to specific applications. The inclusion, adsorption, and occlusion mechanisms that occur during the co-precipitation synthesis technique play main roles in finding the final properties of the material.

2.2.2 Sol-Gel Method

Sol-gel synthesis is a broadly used technique for producing nanostructured materials. This technique involves the formation of a colloidal suspension of tiny solid particles in a liquid, which is called a "sol" and the subsequent transformation of the sol into a solid material called a ‘gel’. The sol-gel process typically involves two main steps: hydrolysis or condensation. In the hydrolysis step, a precursor material is added to liquid, typically water, which breaks the precursor bonds and forms a reactive species. This reactive species then reacts with other precursor molecules, forming a network of interconnected particles. The ongoing reaction then leads to the condensation step, where the particles in the sol begin to bond together to form a solid material. This process of condensation is driven by the removal of water, which serves as a catalyst for the reaction. As the water is removed, the particles in the sol come closer together, forming a gel-like material. The schematic diagram for the synthesis nanomaterials through sol-gel method shown in the figure 2.1.

The sol-gel process offers the substance structure, including the kind of precursor, their concentration, temperature, and PH. These factors can be controlled to create a variety of materials with distinct structures and properties. Producing materials with a high level of purity and uniformity is one of the sol-gel technique's primary benefits. The sol-gel technique can control the form of the particles and filter out pollutants throughout the reaction because it takes place in a liquid environment. In the realm of materials science, sol-gel synthesis has found numerous uses, such as the creation of improved ceramics, glasses, and composites. The

technique is also used in the fabrication of coatings, catalysts, and sensors. Its versatility and ability to produce materials with unique properties make it a valuable tool for researchers and engineers in many different fields.

The sol-gel method is a popular technique for synthesizing oxide nanoparticles due to its convenience and versatility. Reddy and colleagues used the sol-gel method to synthesize a nano-porous V_2O_5. The resulting nano-porous V_2O_5 electrode had a specific surface area of around 7 $m^2 g^{-1}$. The researchers have been able to achieve a specific capacitance of 215 Fg^{-1} in a 2 Mole KCl electrolyte [71].

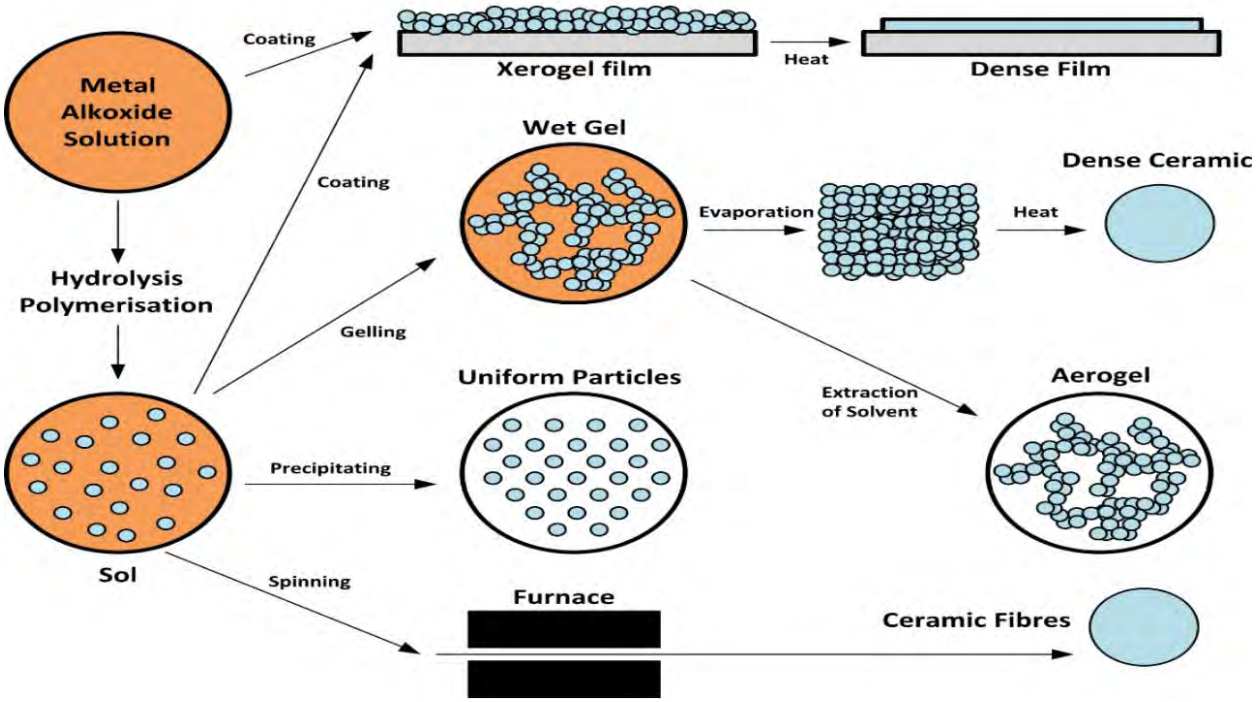

Figure 2.1: Schematic diagram for the synthesis of the sol-gel method [72]

2.3 Synthesis of V_2O_5 Nano structure

Sol-gel synthesis of V_2O_5 nanostructure has been carried out. All of the initial components are of the analytical-grade quality. The synthesis started with the oxalic acid being dissolved in 50 ml of distilled water at a temperature of 60 ºC. After that, 7.018 g of ammonium metavanadate is slowly added to the solution and stirred for 2 hours to yield a blue gel. The blue gel is subsequently dried at 80 ºC for 8 hours and then calcined at 450 ºC in the air for 4 hours.

The production of a stable and crystalline product is favored by the calcination process, which is an essential step in the synthesis of V_2O_5. A yellow V_2O_5 product has been produced once the calcination process has finished. After the calcination process is complete, a yellow-colored V_2O_5 product has been obtained. The formation of V_2O_5 NPs can be attributed to the use of the sol-gel method, which allows for precise control over the size and shape of the particles.

Figure 2.2: Synthesis flow chart of V_2O_5 nanostructure

2.4 Fabrication of V_2O_5-GNPs Nanocomposites

In this experiment, GNPs and V_2O_5 composites have been synthesized using the ex-situ method. The concentrations of the nanocomposites have been varied by mixing 0.75 g of GNPs and 0.25 g of V_2O_5, 0.50 g of each, 0.25 g of GNPs, and 0.75 g of V_2O_5. The mixture is prepared in a motor pistol, and ethanol has been added dropwise during the grinding process, which is lasted for one hour. After fine grinding, the composite is heated at 80ºC for 10 hours. This process is repeated for all the different concentration ratios. The ex-situ method is used in this experiment involves synthesizing the individual composite particles separately and then mixing them, which enables better control over the resulting composite's properties. The principle of this

is experiment is to examine the impact of different concentration ratios of GNPs and V_2O_5 on the resulting composite's properties.

2.5 Nickel Foam Preparation

Nickel foam has been first treated by washing with 3M H_2SO_4, ethanol, and deionized water to remove any oxide layer from the surface before being used as a working electrode. The electrode's active material is prepared, and a thick paste is made by combining 10% carbon black, 10% polyvinylidene difluoride (PVDF), and 80% of the electrode's active material in N-methyl-2-pyrrolidinone (NMP). A nickel foam having a surface area of 1 cm^2 is coated with this paste, which is then dried in an oven at 70 °C for 12 hours to eliminate the solvent. On the nickel foam, an average mass of 2 mg has been deposited. Overall, these actions are done to create a working nickel foam electrode with a homogenous and regulated mass of active material.

Chapter No. 03 Characterization Techniques

3.1 Introduction

Techniques for characterization are crucial for comprehending the characteristics and behavior of supercapacitors. To comprehend the characteristics and functionality of the materials utilized in the device, supercapacitors must be characterized. Four frequently used characterization methods will be discussed in this chapter i.e., energy-dispersive X-ray spectroscopy (EDS), Raman spectroscopy, UV-visible spectroscopy, and X-ray diffraction (XRD). Each method offers distinct details on the supercapacitor's composition and structure, enabling a thorough comprehension of both its characteristics and behavior.

3.2 X-ray diffraction spectroscopy

X-ray diffraction spectroscopy is an effective characterization technique to investigate crystal structure of the materials. The method involves exposing a sample to X-rays and evaluating the resulting diffraction pattern. This pattern, which is a result of crystal structure, can be used to determine the different kinds of crystals that are present in a sample. A non-destructive method for figuring out a material's crystal structure and phase is XRD. It is frequently used to examine single crystals, thin coatings, and powders.

3.2.1 Working Principle

In order for XRD to function, the sample must be exposed to an X-ray beam that is diffracted by the substance crystal structure. The material's crystal structure and phase are then identified by locating and examining the diffracted X-rays. X-ray diffraction (XRD) is a technique for determining the crystal structure of a substance. In order to measure the angles and intensities of the diffracted beams that are scattered in different directions, an X-ray beam is shone upon a sample. The fundamental idea underpinning XRD is that X-rays behave like waves. The atoms in a crystal behave as diffraction gratings when an X-ray beam impacts them scattering the radiation in numerous directions. The viewing angles for the scattered rays and their intensities are related to the arrangement of atoms in the crystal [73]

The XRD procedure are further classified into the following steps:

- To aim the X-ray beam onto various crystal surfaces, the sample is mounted on a holder and rotated. The data is analyzed using software such as Topas, High Score, and Foolproof.
- An X-ray beam is shone onto the sample and the angles and concentrations of the diffracted beams are detected using a detector.
- By comparing the measured diffraction patterns to those of known crystal structures it is possible to find the material crystal structure.
- We can utilize Bragg's Law equation to get the lattice constant (a) and another parameter, such as the unit cell volume (V).

$$\mathbf{n\lambda = 2d \sin \theta} \tag{3.1}$$

Where $\boldsymbol{d}$ is the distance between the atom's planes in the crystal, $\boldsymbol{\lambda}$ is the wavelength of the X-rays, n is the order of diffraction, and θ is the angle of diffraction. We may as certain the values of d and then calculate the lattice constant and unit cell volume, by finding the angles and intensities of the diffracted beams. To create X-rays, three things are necessary.

- An electron sources.
- Highly accelerated electrons.
- The substance that will be the target for the electrons impact and subsequent interaction.

The choice of anode metal, such as Cu, Mo, or Co, can influence the frequency (wavelength) in X-ray generation. Electrons, when ejected from the K shell (n = 1), create spectral lines that are subsequently filled by electrons from higher energy shells. For example, K lines result from electrons transitioning from the L shell (n = 2), and K1 and K2 doublets occur when electrons from the M shell (n = 3) fill the K shell. Typically, a thin metal foil of the adjacent element (Z-1) is employed to select and filter out the K line; for instance, nickel is used to filter the copper K line. Alternatively, specific X-ray beam colors can be chosen by reflecting them from a single crystal plane.

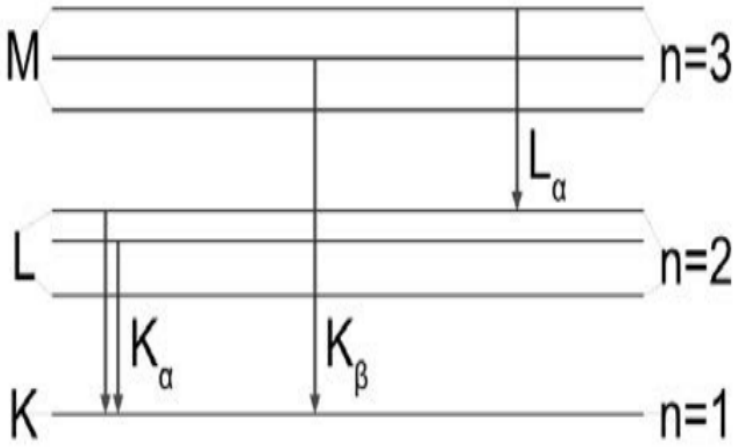

Figure 3.1: Schematic diagram of K_α, K_β lines [74]

3.2.2 Diffraction of X-rays

Crystalline solids are made up of atom, ion, or molecular regular arrays with an interatomic spacing of 100 pm. The wavelength of the incident light must match the atoms' distance from one another. The crystal structures of NaCl, KCl, CaF_2, $CaCO_3$, and diamond were determined by W.L. Bragg. Radiation, including X-rays, reflects only when the conditions necessary for constructive interference are satisfied. [75].

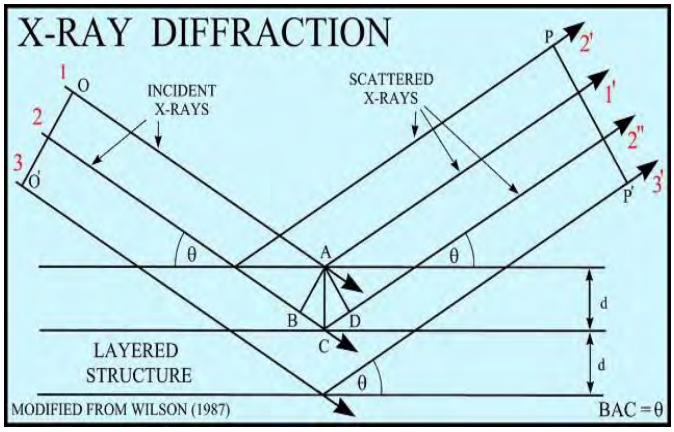

Figure 3.2: Schematic diagram of Diffraction of X-rays [76]

- Path length difference = BC + CD
- BC = CD = $(\sin\theta)_{hkl}\, d_{hkl}$
- Path length difference = $2d_{hkl}\, (\sin\theta)_{hkl}$
- There must be an integral number of wavelengths (n = 1, 2, 3……)

3.2.3 Modern X-ray Diffractometer

A usual method for examining the structure of crystalline materials is X-ray diffraction (XRD). This method is grounded on the idea of X-rays and a crystalline sample interfering constructively. A monochromatic X-ray stream of light is created by filtering the X-rays after they are produced by a cathode ray tube. The beam is then focused onto the sample after being collimated through a small aperture as shown in figure 3.3. When Bragg's law is met, constructive interference between the sample and the incoming X-ray takes place, producing a diffracted ray. Bragg's law links the lattice spacing (d) and diffraction angle ($\boldsymbol{\theta}$) in a crystalline sample to the wavelength ($\boldsymbol{\lambda}$) of electromagnetic radiation. Due to the fact that each mineral is associated with a distinct set of d-spacing, this connection enables the identification of minerals by converting diffraction peaks to d-spacing.

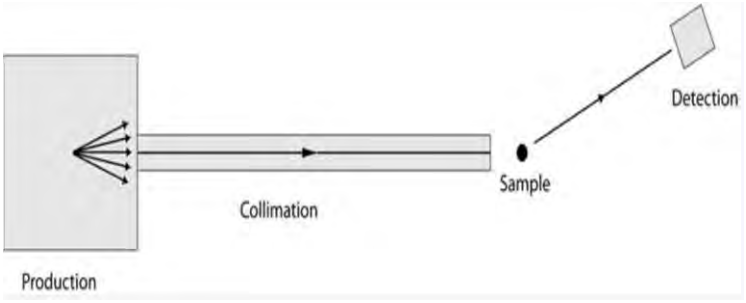

Figure 3.3: Demonstration of basic instrumentation of XRD machine

The size of the material's crystallites is estimated using the Scherrer formula as shown in Equation 4.2. The formula is based on the idea that the size of the crystallites in the sample has an impact on the diffraction peak's width.

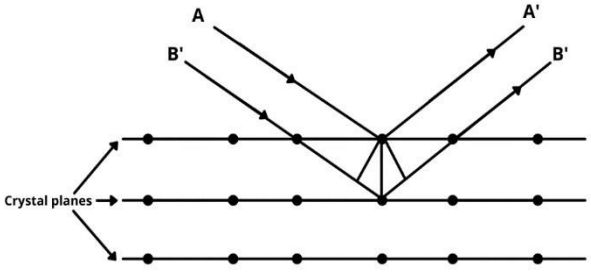

Figure 3.4: A schematic diagram of X-ray diffraction through crystal planes [77]

Modern X-ray diffractometers use advanced technologies to improve the accuracy and efficiency of XRD analysis. The X-ray source in modern diffractometers is typically a sealed tube that generates X-rays through a process called electron bombardment. Modern diffractometers also use a variety of detectors to improve the accuracy and efficiency of XRD analysis. One commonly used detector is the scintillation detector, which is based on the principle of converting X-rays into light. When an X-ray strikes the scintillator material, it produces a burst of light, which is detected by a photomultiplier tube. The crystallite size can be calculated using equation 3.2.

$$\boldsymbol{D} = \frac{0.9\lambda}{\beta\cos\theta} \qquad (3.2)$$

In equation (3.2) "$\boldsymbol{\lambda}$" represents the incident wave wavelength, and "$\boldsymbol{\theta}$" is the incident angle. The crystallite size of the material is calculated by taking the means of all the calculated crystallite size values of the prominent peaks in the XRD pattern. Lattice parameters for different crystal symmetries can be obtained by using a relation that relates plane spacing, miller indices, and lattice parameters. For rhombohedral crystal structure, the prescribed relation can be written as (3.3)

$$\frac{\mathbf{1}}{\boldsymbol{d_{hkl}^2}} = [\frac{\mathbf{4}}{\mathbf{3}}(\boldsymbol{h^2 + k^2 + hk}) + \boldsymbol{l^2}(\frac{\boldsymbol{a^2}}{\boldsymbol{c^2}})]\frac{\mathbf{1}}{\boldsymbol{a^2}} \qquad (3.3)$$

Equation (3.3) along with equation (3.2) has been used to calculate the lattice parameters for the rhombohedral structure of the material. Calculating lattice constant, a can be done by the use of the following formula (3.4).

$$\boldsymbol{a} = \frac{\mathbf{4}}{\mathbf{3}}\boldsymbol{d^2}((\boldsymbol{h^2 + k^2 + hk}) \qquad (3.4)$$

Where “d” indicates the d-spacing and also lattice parameter “a” is equivalent to lattice parameter “b”. Lattice parameter “c” is calculated using the following formula.

$$\boldsymbol{c} = \sqrt{\frac{\boldsymbol{l^2}}{\frac{\mathbf{1}}{\boldsymbol{d^2}} - \frac{\frac{\mathbf{4}}{\mathbf{3}}(\boldsymbol{h^2+hk+k^2})}{\boldsymbol{a^2}}}}$$

The crystallite Volume is calculated using the given equation.

$$\mathbf{V}=\frac{\sqrt{\mathbf{3}}}{\mathbf{2}}\boldsymbol{a^2 c} \qquad (3.5)$$

Where “a” and “C” is the “Lattice Parameters”, and “V” is the volume of crystallite.

3.3 Raman Spectroscopy

3.3.1 Introduction

An effective analytical method for examining the rotations and vibrations of molecules is called Raman spectroscopy. It is based on the Raman phenomenon, which is a molecule's inelastic light scattering. The polarizability of the molecules interacts with light to produce the Raman effect, which results in the scattered light having a different frequency from the input light. The Raman shift is the difference in frequency between the incident light and the dispersed light, and it is specific to the vibrational and rotational modes of the molecule. Many fields, including chemistry, biology, materials science, and geology, employ Raman spectroscopy extensively to identify and research various sorts of chemicals, and analyze complex mixtures [78].

3.3.2 Working Principle

When a molecule is exposed to monochromatic light from a laser or other light source, some of the light scattered by the molecule will have an equal frequency as the incident light, while other light will have a different frequency.

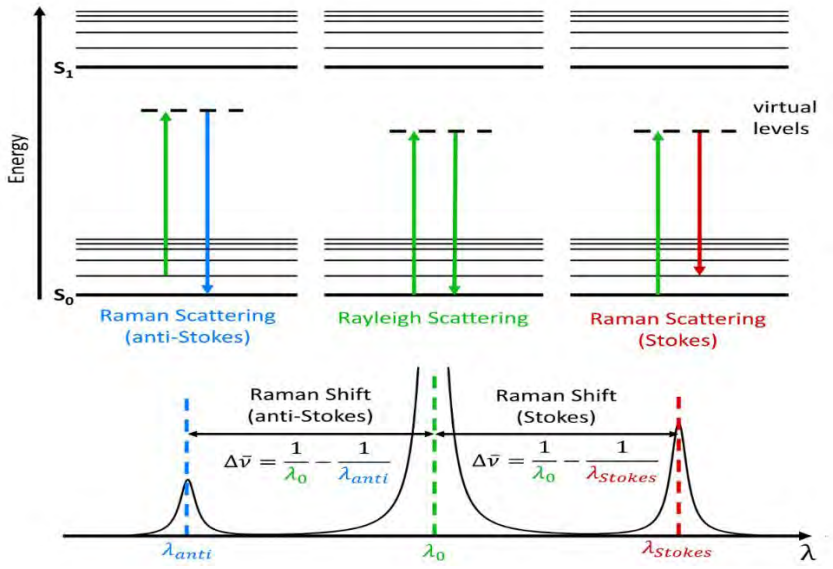

Figure 3.5: Schematic diagram for Raman spectroscopy [79]

Raman spectroscopy normally makes use of a strong laser and a sensitive detector to detect the scattered light because the Raman effect is quite faint. The intensity of the dispersed light is plotted against the Raman shift to get the Raman spectrum as shown in figure 3.5. Different experimental setups, including transmission, reflection, and fluorescence, can make use of Raman spectroscopy. The kind of sample and the information sought-after determine the experimental configuration to be used. It is possible to identify unknown compounds, examine the conformation of biological macromolecules, and characterize the structure of minerals and other materials using the information contained in the Raman spectrum, which carries information about the chemical composition, structure, and bonding of the molecule [80]. In conclusion, Raman spectroscopy is an analytical method that studies the rotations and vibrations of molecules using the Raman effect and can provide details about their chemical makeup, structure, and bonding. Raman spectroscopy is a non-destructive, non-invasive method that may be used to examine a variety of materials and has numerous uses in numerous disciplines.

3.4 UV-Visible Spectroscopy

A common analytical method that permits the identification and quantification of chemicals in a sample is UV-Visible spectroscopy. It works on the premise that molecules absorb light at particular wavelengths that are distinctive to their chemical composition. The absorbing species in the sample directly relates to the amount of light that is absorbed. The UV-Visible Spectrophotometer, the tool used to do this analysis, will be the subject of discussion in this article.

3.4.1 Working Principle of UV-Visible Spectrophotometer

The operation of UV-Visible Spectrophotometers is based on the Beer-Lambert equation, which connects the concentration of an absorbing species in a solution to the amount of light that species absorbs. The rule states that the concentration of the absorbing species and the length of the light passage through a solution are inversely proportional to each other. The path length is the distance that light travels through the sample. The UV-Visible Spectrophotometer uses a monochromatic light beam with a wavelength that varies from 200 nm to 800 nm to detect the amount of light that is absorbed by a sample. In this technique, two lamps are used i.e., a tungsten lamp for the visible spectrum and a hydrogen or deuterium light for the UV spectrum. The sample is often put in a tiny cuvette, which is a clear glass or plastic container. The instrument uses two cells a reference cell and a sample cell. While the sample cell contains

the solution of interest, the reference cell contains a solvent that does not absorb light at the wavelength of interest. The reference cell acts as the instrument's baseline, and any variations in the sample cell absorbance are contrasted with it.

A beam splitter divides the monochromatic beam of light into many beams as it travels through the device. Both beams travel through the sample cell and the reference cell, respectively. While light that passes through the reference cell is not absorbed, light that permits through the sample cell is absorbed by the sample. A detector then gathers the light that has been delivered from both cells [81]. A photodiode or a photomultiplier tube is commonly used as the instrument's detector. It transforms the transmitted light's intensity into an electrical signal, which the instrument processes after measuring it. The gadget calculates the sample's absorbance by comparing the intensity of transmitted light from the sample cell to the intensity of transmitted light from the reference cell. The sample's spectrum is created by plotting the sample's absorbance against the light's wavelength. The sample's chemical composition and concentration can be determined from the spectrum, which is a graphic depiction of the sample's absorbance at various wavelengths.

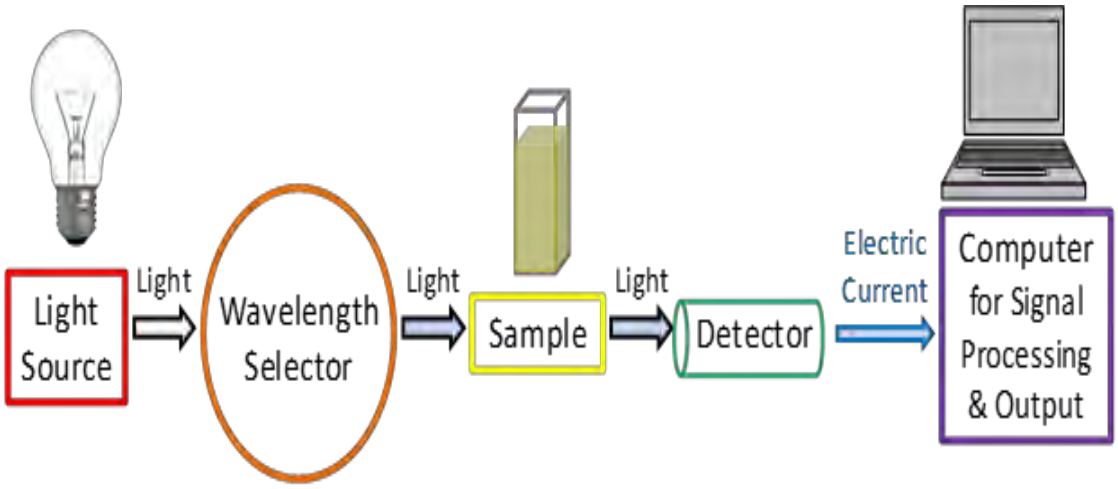

Figure 3.6: UV-Visible spectroscopy set-up [82]

3.5 Scanning Electron Microscope (SEM)

The Scanning Electron Microscope (SEM) was developed in the early 1940 to visualize objects at a microscopic level with high magnification and resolution. The electron microscope allows for direct visualization and morphological explanation of samples, making it possible to observe objects at a microscopic level. The SEM uses the wave nature of electrons to observe the sample, and different interactions occur when an electron beam interacts with the sample. These interactions include scattering, diffraction, and tunneling through the material, which give valuable information on the crystal structure, of the sample. In summary, the SEM is an essential tool in microscopy, allowing scientists to observe and analyze samples at a microscopic level, providing invaluable insights into their morphology and structure.

3.5.1 Working Principle of SEM

The SEM operates on the basic principle of electron scattering. The instrument emits an electron beam via thermionic emission from a tungsten filament, which is then accelerated through a high voltage, typically 21 VK, before passing through various optical systems. They scan the surface of the sample, which emits electrons from its surface and is detected by different detectors in the chamber. The SEM relies on several sources, including the electron gun, condenser lenses, objective aperture, scan coils, chamber, and detectors. In thermionic emission, electrons are emitted by applying thermal energy to the filament, while in a field emission gun, a strong electric field is generated to emit electrons. The condenser lenses control the electron beam, allowing for thin and fine adjustments to produce clear images. An objective aperture is a thin metallic sheet with four holes held by a small rod, which allows for the selection of a hole of any size to pass the electron beam.

The scan coil consists of two solenoid coils, with the current in one coil changing the magnetic field in the other and vice versa. The scan coil is used to scan the sample in the specimen and provides results using different detectors, including the secondary electron emission detector, backscattered detector, X-ray emission detector, and Auger electron emission detector [83]. When the basic electron beam strikes a sample, the secondary electron emission detector is utilized to gather the electrons that are released from the sample's surface. The backscattered detector, which detects the intensity of the electrons that are scattered back from the sample surface, establishes the atomic number and density of the sample. X-ray emission detector is used to measure the X-rays that are emitted when the electron beam hits the sample in

order to ascertain its chemical composition. The surface of the sample emits electrons when it is hit by the primary electron beam, which are subsequently detected by the Auger electron emission detector.

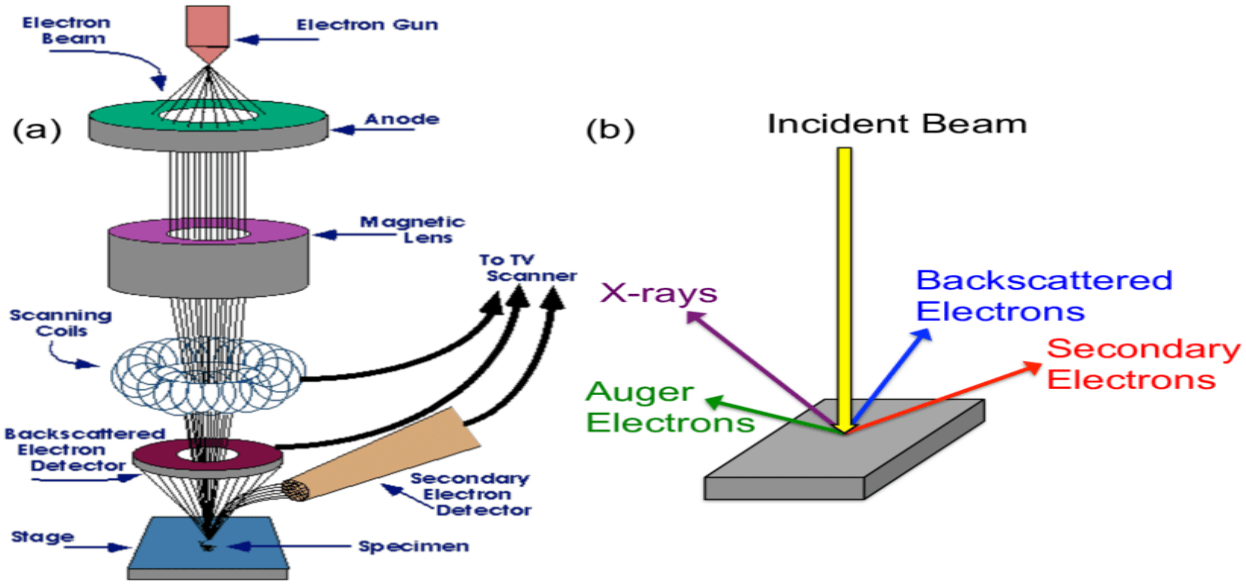

Figure 3.7: Schematic diagram of SEM [84]

3.6 Fourier Transform Infrared Spectroscopy

3.6.1 Introduction

The effective analytical technique known as Fourier Transform Infrared Spectroscopy (FTIR) is used to identify and characterize both organic and inorganic compounds. It offers useful details on the molecular makeup, functional groups, and chemical make-up of a variety of materials. An in-depth description of FTIR and its operating principle is the goal of this note.

3.6.2 Working Principles

The interaction of infrared radiation with molecules forms the basis for the operation of FTIR. Specific infrared light frequencies that match to the vibrational modes of the atoms that make up molecules are absorbed by them. Some infrared wavelengths are absorbed when they hit a sample, whereas others are transmitted or reflected. FTIR can be used to analyze the absorbed wavelengths and reveal important details about the molecular makeup of the sample.

3.6.3 Instrumentation

Broadband infrared radiation is produced by an infrared source, most frequently a heated filament, a globar (silicon carbide rod), or a carbon dioxide laser. The source radiates at a

number of different frequencies. Using a beam splitter, infrared energy is separated into two beams. It typically makes use of a substance that, based on its optical properties, transmits, and reflects radiation, such as potassium bromide (KBr) or calcium fluoride (CaF_2). The sample compartment is where the sample that will be examined is kept.

3.6.4 Working Process

The following steps are included in the FTIR working process:

- A wide range of infrared radiation is emitted by the infrared source.
- While the reference beam avoids the sample, the sample beam travels through the sample compartment and interacts with the sample.
- After interacting with the sample and reference, respectively, the two beams are merged once more at the detector.
- An interferogram, produced by the interferometer, shows how the two beams interfere with one another.
- Using the Fourier transform, the interferogram is transformed into a spectrum.
- To evaluate the sample's molecular makeup and structure, the resulting spectrum is examined for recognizable absorption peaks.

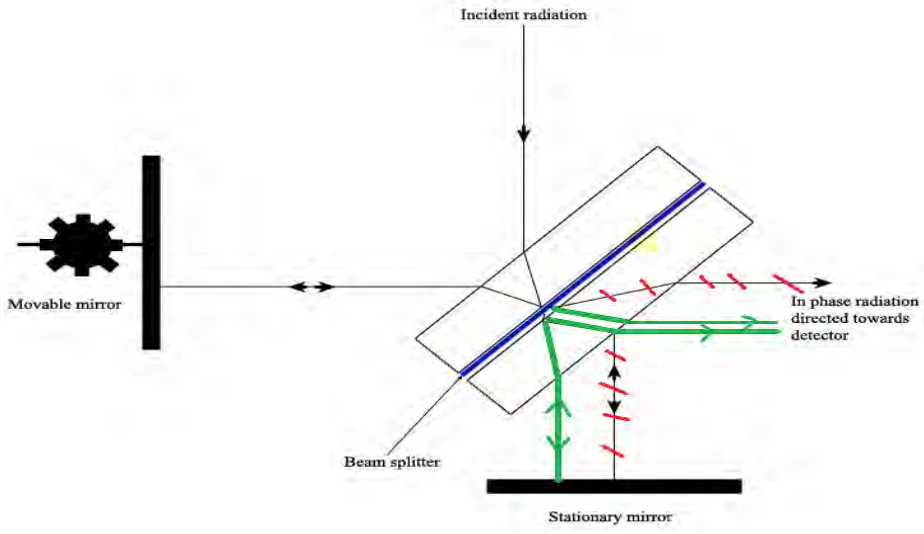

Figure 3.8: Schematic diagram of FTIR

3.7 Electrochemical Measurements

3.7.1 Electrochemical Study

Electrochemistry is the scientific study of the processes involved in energy storage devices that utilize both chemistry and physics. This field of study focuses on both faradaic and non-faradaic electrochemical phenomena that occur due to the conduction of electrons and ions. Electron conductivity occurs when electrons move between electrodes, while ion conduction involves the electrolyte facilitating the movement of ions. Electrodes are usually solid, but they can also consist of liquid and air phases, while electrolytes can be liquid or semi-solid in the form of a paste. Understanding electrochemical processes is critical for designing and optimizing energy storage devices, like batteries, and fuel cells.

3.7.2 Work Station

The electrochemical analysis is a critical process used to measure the chemical reactions that occur within a system when an electric current is passed through it. This analysis is carried out using an electrochemical workstation, such as the Gamry Potentiostat, which is made up of different electrode systems. The workstation can perform various electrochemical measurements that are useful in energy storage applications. The most common electrode system used in electrochemical analysis is the three-electrode system, consisting of the reference, counter, and working electrodes. The counter electrode is often made of platinum wire, while the reference electrode is typically made of Ag/AgCl, $HgCl_2$, or calomel. The working electrode is made up of understudy active materials that are commonly deposited on the surface of a substrate that acts as a support.

The electrochemical workstation can run in different modes, but the most important are the Galvano-static and Potentiostatic modes. A potential is applied across the working electrode and reference electrode during Potentiostatic measurements, and the amount of circulating current between the working electrode and counter electrode is tracked. Galvanostatic measures, on the other hand, give a current across the working electrode and counter electrode while measuring the voltage across the reference electrode and the working electrode.

The two-electrode configuration is another system used in electrochemical analysis, which differs slightly from the three-electrode system. In this configuration, the counter electrode is linked to the reference electrode. The two-electrode system can be categorized as either the

asymmetric electrode system or symmetric electrode system, depending on whether the electrodes are composed of the same material or two distinct materials. Both systems are efficient in illustrating the actual specific energy and specific power quite accurately.

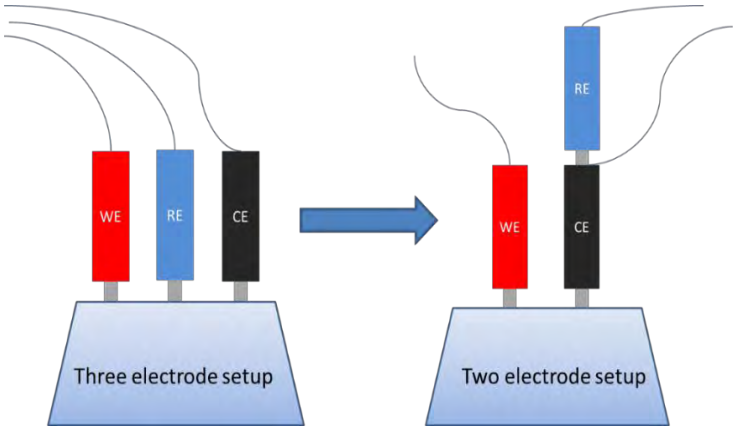

Figure 3.9: Three electrodes system, and two electrodes system [85]

3.7 Electrochemical Characterization

Characterization of the Electrochemical to assess the performance of electrodes in diverse applications, including lithium-sulfur (Li-S) batteries and supercapacitors, electrochemical characterization techniques are crucial. Among the principal electrochemical methods employed for this purpose are cyclic voltammetry (CV), Galvano-static charge-discharge measurements (GCD), and electrochemical impedance spectroscopy (EIS).

3.7.1 Cyclic Voltammetry (CV)

Numerous electrochemical techniques are used to analyze various redox processes, including cyclic voltammetry. In supercapacitors as well as coin cells, it is utilized to assess the stability of reaction products and the presence of intermediates in oxidation-reduction reactions. Cathodic and anodic peaks are two pairs of peaks that can be seen during a redox reaction. When the potential of a working electrode is cycled at a specific scan rate, the response current is measured. A typical cyclic voltammetry experiment consists of an electrochemical cell with a working electrode, a reference electrode, and a counter electrode. The redox reaction of interest occurs at the working electrode, which is typically constructed of a conductive substance (such as a metal or a carbon-based material). The working electrode's potential is measured against a stable reference potential provided by the reference electrode. The working electrode and reference electrode can exchange current thanks to the counter electrode, which completes the electrical circuit. An ammeter is used to measure the resulting current (current density) while the

potential is swept. Information about the electrochemical activities taking place at the working electrode can be gleaned from the amplitude and direction of the current. Due to the movement of electrons during oxidation and reduction reactions, electricity flows.

3.7.2 Galvanostatic Charge-Discharge (GCD)

Galvanostatic charge-discharge is considered to be the most common method for assessing the efficiency of energy storage devices, especially supercapacitors. The two most frequently employed modes are Galvano-static charge-discharge (GCD) and potentiostatic charge-discharge (PCD). During PCD measurements, the current value is monitored at a given voltage. Conversely, in the GCD mode, the voltage magnitude is monitored while providing a constant current in the scanning process. The GCD mode is used in this work to measure capacitance (Csp), energy density (ED), power density (PD), and cyclic behavior utilizing a three-electrode as well as two-electrode system in a symmetric manner.

3.7.3 Electrochemical Impedance Spectroscopy (EIS)

The reaction in electrochemical processes in energy storage devices is studied using a technique called electrochemical impedance spectroscopy (EIS). The conceptual model for EIS was developed by Oliver Heaviside from 1880 to 1900. He investigated how inductors, capacitors, and other electric constituents work within circuits to conduct electrical currents. EIS is used to assess a coin cell's internal resistance, which includes the electrolyte resistance, charge transfer resistance, and interface resistance. The high-frequency semicircle in the EIS spectrum, which denotes the double-layer capacitance and the charge transfer resistance, is tied to the kinetic processes. Lithium ions' solid-state migration into the majority of the active materials is reflected in the low-frequency linear tail. He defined terminology like admittance, impedance (Z), and reactance. The EIS behavior of energy storage materials may be explained using EIS data, which might be made up of several phases like modulus, Nyquist phase, and bode phase. By placing real resistance on the X-axis and imaginary resistance on the Y-axis, the Nyquist plot is created. The charge transfer resistance at the high-frequency zone can be calculated using the radius of the semicircle.

The performance of electrodes in energy storage devices must be assessed using electrochemical characterization methods such as cyclic voltammetry, Galvano-static charge-discharge tests, and electrochemical impedance spectroscopy. These methods help in

understanding the kinetic processes and internal resistance of the apparatuses, which are essential components in the creation of effective energy storage devices.

Chapter No.04 Results and Discussion

4.1 Structural Studies

The structural properties and phase formation of V_2O_5, GNPs, and V_2O_5-GNPs (GNPs) nanocomposites have been studied at room temperature using X-ray diffraction (XRD) technique as shown in the figure 4.1. The results have revealed that V_2O_5 has different mean peaks with high intensity located at 2θ = 20º, 21.3º, 26.1º, 31º, 32.50º, 41.23º, 45.45º, 47.50º, and 51º with corresponding crystal planes (001), (101), (110), (301), (011), (002), (411), and (600). All peaks are well index with the standard (JCPD) data card number (00-041-1426) as shown in Figure 4.1 [86]. The presence of graphene (GNPs) in the NCs has been confirmed by the observation of characteristic peaks in the X-ray diffraction (XRD) patterns. Specifically, three peaks corresponding to the lattice planes of (002), (100), and (004) of GNPs are observed at 2θ angles of 26.8º, 42.64º, and 54.89º, respectively. The XRD patterns shown in figure 4.1 is in good agreement with the JCPDS Card no (00-008-0415), which is a standard reference for the purity of GNPs.

Figure 4.1: X-ray diffraction pattern of V_2O_5 NPs

The Deby Scherrer formula and lattice parameters equations 4.1 and 4.2 have been used to determine the crystallite sizes and lattice parameters of material.

$$D = \frac{0.94\lambda}{\beta\cos\theta} \quad (4.1)$$

The Deby Scherrer formula "λ" calculates the average crystallite size of a material by considering the wavelength of the “Cu-Kα” source, “FWHM” in radians, and “Bragg's angle”.

$$a = d\sqrt{h^2 + k^2 + l^2} \quad (4.2)$$

Equation 4.2 determines the lattice parameter constants of the material using the miller indices, spacing between interplane, and the value of 'd'. The spacing between interplanes is calculated using the miller indices, and the lattice parameter constants are determined by multiplying the interplanar spacing with the square root of the sum of squares of the miller indices. The calculated parameters are given in table 4.1.

Figure 4.2: X-ray diffraction pattern of GNPs

Table 4.1. The vales of different structural parameters

Nanocomposite	Position (2θ)	FWHM (2θ)	Lattice spacing (d_{hkl})	Lattice constant (a)	Unit cell volume (10^6 pm^3) Å^3	Crystallite size (Å)	Density ρ (g/cm^3)	Specific surface area (m^2/g)
V_2O_5	26.03	0.20	3.42	11.51	179.5	416	3.32	43.44
$(V_2O_5)_{0.25}(GNPs)_{0.75}$	26.47	0.23	3.36	11.51	179.5	358	3.32	50.48
$(V_2O_5)_{0.50}(GNPs)_{0.50}$	26.21	0.62	3.40	11.51	179.5	131	3.32	137.9
$(V_2O_5)_{0.75}(GNPs)_{0.25}$	26.01	0.19	3.42	11.51	179.5	431	3.32	41.93
GNPs	26.14	0.48	3.40	2.47	35.54	173	2.16	26.70

Moreover, the XRD patterns have shown that the intensity of the GNPs peaks is increased with higher ratios of GNPs substitution in the NCs. This indicates that the GNPs are successfully incorporated into the NCs.

The presence of GNPs diffractions in different patterns of NCs with different stoichiometric ratios can be observed. The XRD patterns confirm the successful formation of $(V_2O_5)1\text{-}x\text{-}(GNPs)x$ (x= 0.75, 0.50, 0.25) NCs, as evidenced by the presence of both GNPs and host material peaks in the patterns. The XRD patterns also reveal that the GNPs content increased, the crystallite size of the NCs decreased. The crystalline size of $(V_2O_5)_{0.50}$-$(GNPs)_{0.50}$ is found to be 131 Å which is lower than all other nanocomposites and pure NPs as shown in the table 4.1.

This decrease in the crystallite size can directly defects on the surface of the V_2O_5. This shows the successful incorporation of GNPs into NCs containing V_2O_5, as confirmed by XRD patterns. The intensity of the GNPs peaks in the patterns increases with higher ratios of GNPs substitution in the NCs, increasing GNPs content crystallite size of the NPs decreases as shown in table 4.1. The decrease in crystalline size in a nanocomposite is due to combination of interface and strain effects, agglomeration, prevention of crystal growth. When GNPs is added to V_2O_5 NPs, the XRD peaks shift to higher angles and become broader as shown in figure 4.3 (a-d). This can be due to various factors such as strain effects caused by differences in lattice constants, changes in particle size affecting crystalline domains, microstructural alterations, particle clustering, potential solid solution formation, chemical interactions, stress effects from thermal expansion differences, and surface interactions between GNPs and V_2O_5.

Figure 4.3: X-ray diffraction patterns a) V_2O_5 b) $(V_2O_5)_{0.25}(GNPs)_{0.75}$ c) $(V_2O_5)_{0.50}(GNPs)_{0.50}$ d) $(V_2O_5)_{0.75}(GNPs)_{0.25}$ e) GNP

To validate the findings based on the morphology, the surface area can be found from XRD analysis as shown in Table 4.1. The results indicated that the surface area of V_2O_5, $(V_2O_5)_{0.25}GNPs_{0.75}$, $(V_2O_5)_{0.75}GNPs_{0.25}$, and GNPs was 43.44 m^2/g, 50.48 m^2/g, 41.93 m^2/g, and 26.7 m^2/g respectively. The addition of GNPs well enhances the surface area i.e., $(V_2O_5)_{0.50}$ $GNPs_{0.50}$ showed a surface area of 137.9 m^2/g, due to the aggregation of V_2O_5 blocks with graphene, which was almost four to five-time greater than the surface area from all other composites. These results demonstrate that the specific surface area of the material can significantly increase after the addition of GNPs. Moreover, it has been observed that the growth rate of the specific surface area reduces as the number of GNPs added increases. The crystalline size is also decreased with an increase in the GNPs concentration and is found 131 Å of a $(V_2O_5)_{0.50}GNPs_{0.50,}$ which is almost three times less than pure V_2O_5 as shown in Table 4.1. The surface area available for electrochemical reactions is greatly increased by decreasing the crystalline size of a nanocomposite material used in supercapacitors. The better ion adsorption and desorption kinetics encouraged by the higher surface area result in increased capacity for charge storage. A higher power density is also made possible in the supercapacitor by the larger surface area, which further speeds up ion diffusion within the material. Overall, these advantages

result in better energy storage, quicker charge/discharge rates, and higher supercapacitor efficiency for a variety of applications.

Overall, the results suggest that the XRD technique is used to determine the structural properties and phase formation of V_2O_5, GNPs, and V_2O_5/GNPs nanocomposites at room temperature. The presence of well-matched peaks with standard (JCPD) data card numbers confirms the purity of the samples, while the broadening of peaks and shifts in peak position suggests the introduction of defects and strains resulting from the addition of oxides in the composite samples. These findings have important implications for the development of new materials with improved structural properties and may guide the design of future studies aimed at optimizing the properties of V_2O_5, GNPs, and V_2O_5-GNPs nanocomposites.

4.2 Vibrational Studies

FTIR analysis tell us about the Vibrational modes of V_2O_5 and their nanocomposites. FTIR spectra in the 400–4000 cm^{-1} region are obtained using a KBr pellet as a reference for Fourier transformation. Figure 4.4 displays the FTIR transmittance spectra of the vibration modes for V_2O_5, GNPs, and $(V_2O_5)_{0.50}(GNPs)_{0.50}$. O-H and H-O-H motifs may appear in $(V_2O_5)_{0.50}(GNPs)_{0.50}$ as a result of the intermediate product GNPs.

Figure 4.4: FTIR spectra a) V_2O_5 b) $(V_2O_5)_{0.50}(GNPs)_{0.50}$ c) GNPs

The FTIR spectra are recorded for the precursor substance employed in the experiment. GNPs show bands that are frequency-wise related to those of $(V_2O_5)_{0.50}$-$(GNPs)_{0.50}$ [87]. For GNPs and $(V_2O_5)_{0.50}(GNPs)_{0.50}$, the Sp_2 hybridized C=C in-plane vibration peaks at 1761 cm-1. Around 1003 cm^{-1} of V=O stretching mode occurs in pure V_2O_5. V-O-V stretching mode corresponds to the peaks at 827 cm^{-1} and 594 cm^{-1}. Common V=O and V-O-V peaks in the case of $(V_2O_5)_{0.50}(GNPs)_{0.50}$ can be seen at 927, 692, and 502 cm^{-1} respectively. Peaks' downward movement suggests a strong interaction between V_2O_5 NPs and GNPs layers [88].

4.3 Optical Studies

The optical properties of $(V_2O_5)1\text{-}x(GNPs)x$ nanocomposites (where x = 1, 0.75, 0.50, 0.25, 0) have been investigated by UV-vis absorption spectroscopy as shown in the figure 4.5. Materials for electrochemical applications must have certain optical characteristics. The absorption peak in a pure sample of GNPs, and V_2O_5 is 238 nm, and 258 respectively is shown in (Fig. 4.5). For $(V_2O_5)1\text{-}x(GNPs)x$ (where x = 1, 0.75, 0.50, 0.25, 0) compositions, the absorption peak changes slightly towards shorter wavelengths at 254, 245, and 252 nm, respectively when x decreases (x = 0.75, 0.50, and 0.25) as shown in the figure 4.5 (a-e). The creation of a single phase is confirmed by the existence of a single peak in all spectra, which also validates the findings of XRD and SEM about the phase purity of the samples. The Tauc relation, $\boldsymbol{\alpha h\upsilon = \beta (h\upsilon - E_g)^n}$ have been used to decide the optical band gap energy for nanocomposites, and the results are shown in Fig. 4.5. The absorption edge of a semiconductor materials is frequently described by the Tauc relation. The sort of transition occurring inside the band structure of the material determines the value of "n". "n" takes on the value of 1/2 for indirect allowed transitions and the value of 2 for direct allowed transitions. According to numerous reports, [89] V_2O_5 and GNPs have indirect band gaps, hence the band gap energies E_g have been obtained by drawing a tangent to the root of absorbance time energy along the y-axis $((\alpha h\nu)^{1/2})$ and energy along the x-axis ((hv)) with n=1/2. E_g are calculated to be 2.80 eV and 3.14 eV, respectively, for V_2O_5 and GNPs as shown in figure 4.5. For intermediate compositions of $(V_2O_5)1\text{-}x(GNPs)x$ nanocomposites (where x = 0.75, 0.50, 0.25), band gap energies are 2.9 eV, 2.38 eV, 2.34 eV, respectively as shown in the figure 4.5(b-d). The Ragone plot between E_g verse sample code is shown in Figure 4.5(f). The addition of graphene caused a narrowing of the band gap energy of V_2O_5, which could be affected to several factors, such as smaller crystallite sizes, the establishment of a localized state between the valence bands and conduction bands of oxides,

presence of strain, oxygen vacancies and quantum confinement [90]. Overall, the results demonstrate that intermediate nanocomposites optical band gaps have been tunned, demonstrating their semiconductor character.

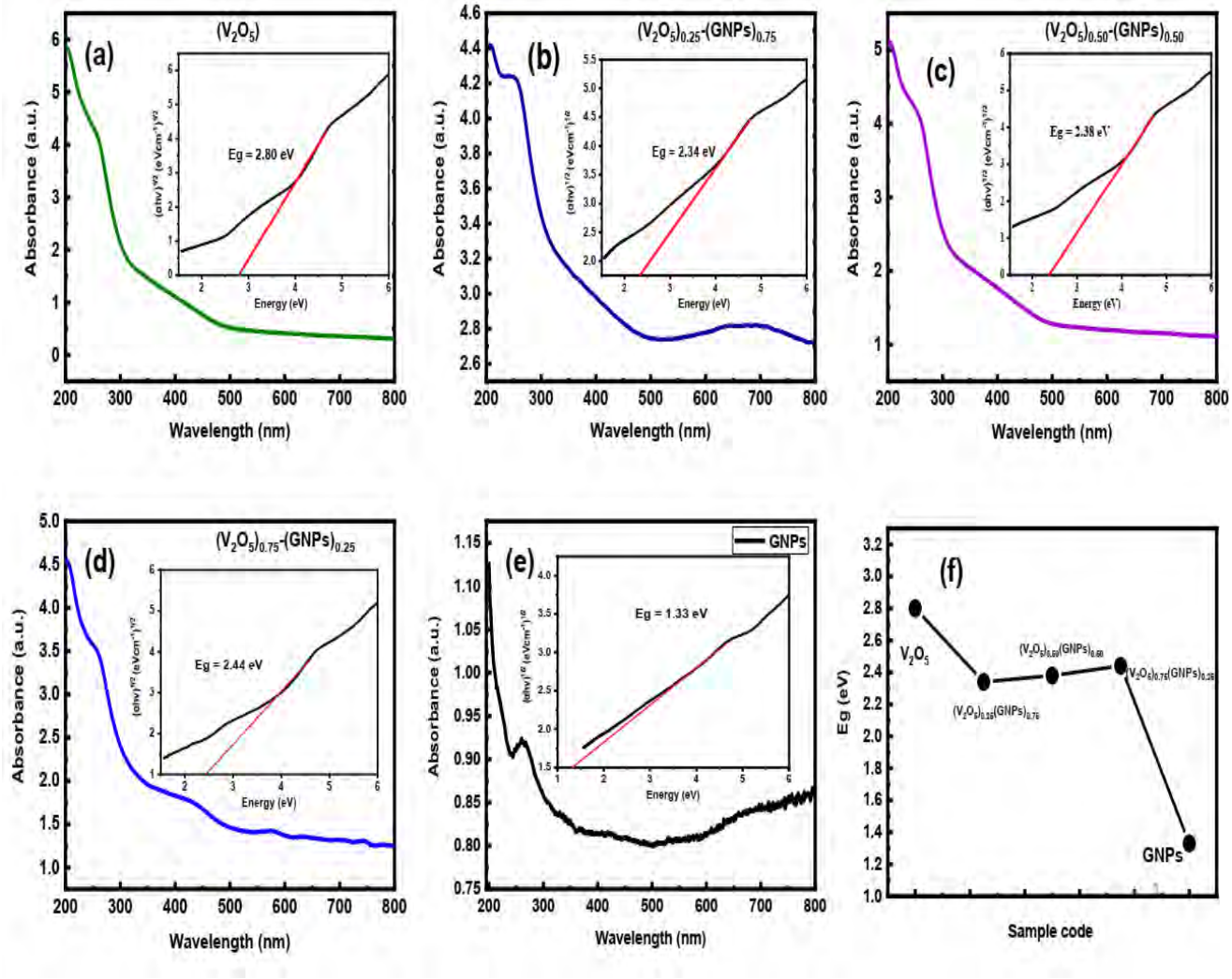

Figure 4.5: Tauc's plots of a) V_2O_5b) $(V_2O_5)_{0.25}(GNPs)_{0.75}$ c) $(V_2O_5)_{0.50}(GNPs)_{0.50}$ d) $(V_2O_5)_{0.75}$ $(GNPs)_{0.25}$ e) V_2O_5, and f) Ragone plot of E_g as a function of sample code

The addition of GNPs has also tailored the optical bandgap of V_2O_5 toward the visible region, which has the potential for solar light-triggered energy-efficient devices. This trend of bandgap tailoring as a function of graphene concentration with the host matrix is shown in Figure 4.5 (a-e). These visible-light bandgap nanomaterials have potential applications in photocatalysis, LEDs, and supercapacitors. Overall, this study provides effective insights into the properties and potential applications of V_2O_5, GNPs, and their nanocomposites. The ability to

tailor the band gap energy of these materials through the addition of GNPs opens up new possibilities for the cost-effective and efficient development solar energy conversion technologies.

4.4 Electrochemical Studies

4.4.1 Cyclic Voltammetry (CV)

A typical technique cyclic voltammetry (CV) is used for examining the electrochemical behavior of materials. In this study, $(V_2O_5)1\text{-}x(GNPs)x$ (x= 1, 0.75, 0.50, 0.25, 0) nanocomposites have been subjected to CV tests to assess their suitability as supercapacitor electrode materials. A three-electrodes setup has been used to evaluate the nanocomposites. The Nickel foam, Ag-AgCl, and Platinum wire are used as working, reference, and counter electrode respectfully. 2M solution of NaOH is used as electrolyte in experiment. For a chosen potential window (0.0 to 0.7 V), the CV curves have been scanned between 5-100 mV/s. Equation 4.4 is used to determine the specific capacitance of the synthesized composite material based on the voltage window that is chosen (V), the area of the CV curve (A), the mass of active materials (m), and the scan rate (k).

$$C_s = \frac{A}{\mathbf{mK\Delta V}} \qquad (4.4)$$

The nanocomposite is made of 50% GNPs and Vanadium pentoxide (V_2O_5), which has a significantly higher specific capacitance of 1193 F g^{-1} as compared to the individual components of V_2O_5 (676 F/g) and GNPs (233 F/g). The ragone plot of specific capacitance as a function Scan rate is shown in the figure 4.6 (g).This improvement in specific capacitance is due of conducting nature of GNPs. V_2O_5 have insulating nature which is increase by the conductive nature of GNPs.

The synergistic interaction between the 2D GNPs and the 1D V_2O_5 NPs is responsible for the increase in the specific capacitance of the nanocomposites. These two components are in closer contact with one another when combined, which increases the composite's conductivity. The V_2O_5 NPs are connected by graphene nanoplates, which boosts the conductivity of the composite. The redox activity of the nanocomposite is improved as a result of the enhanced conductivity. Another reason for boosting the conductivity of the nanocomposite is due to the high conductivity of graphene. Graphene has a high electrical conductivity because of its unique electronic structure, which allows electrons to move through the material with minimal

resistance. This high conductivity of graphene provides a pathway for electrons to flow through the nanocomposite, improving its overall conductivity [91-92].

When the scan rate is increased from 5 to 100 mV/s, it is observed that the specific capacitance of the nanocomposites is decreased as shown in the Table 4.2. Reduced capacitance is the result of the ions' insufficient time to get to the inner layer of the active materials, which is the cause of this trend. The shape of the CV curves of pure V_2O_5 and their NCs show the existence of redox peaks serve as indicators that the nanocomposites exhibit pseudocapacitive behavior as shown in the figure 4.6 (a-d). The presence of a redox peak in the cyclic voltammetry graph of V_2O_5 within the potential range of 0.35-0.5V indicates reversible electrochemical reactions involving vanadium ions.

Table 4.2. Specific capacitance values obtained from Cyclic Voltammetry (CV).

Scan rate (K)	**Specific capacitance (Cs) F g^{-1}**				
mV s^{-1}	**V_2O_5**	**$(V_2O_5)_{0.25}(GNPs)_{0.75}$**	**$(V_2O_5)_{0.50}(GNPs)_{0.50}$**	**$(V_2O_5)_{0.75}(GNPs)_{0.25}$**	**GNPs**
100	183	327	476	267	103
75	219	365	554	313	123
50	251	417	640	374	136
20	418	642	882	600	160
10	472	640	1030	650	183
5	676	908	1193	683	233

These reactions could involve vanadium's different oxidation states, intercalation and deintercalation of ions in energy storage systems, oxygen evolution and reduction, electrochemical conversion, or reversible adsorption/desorption processes [93]. The shape of a CV curve of pure GNPs does not show any redox peak which conform that the GNPs have EDLC behavior as shown in the figure 4.6 (f). The oxidation peak advances towards the positive electrode as the scanning rate increases, whereas the reduction peak moves towards the negative electrode. This result reveals the electrode material's internal resistance.

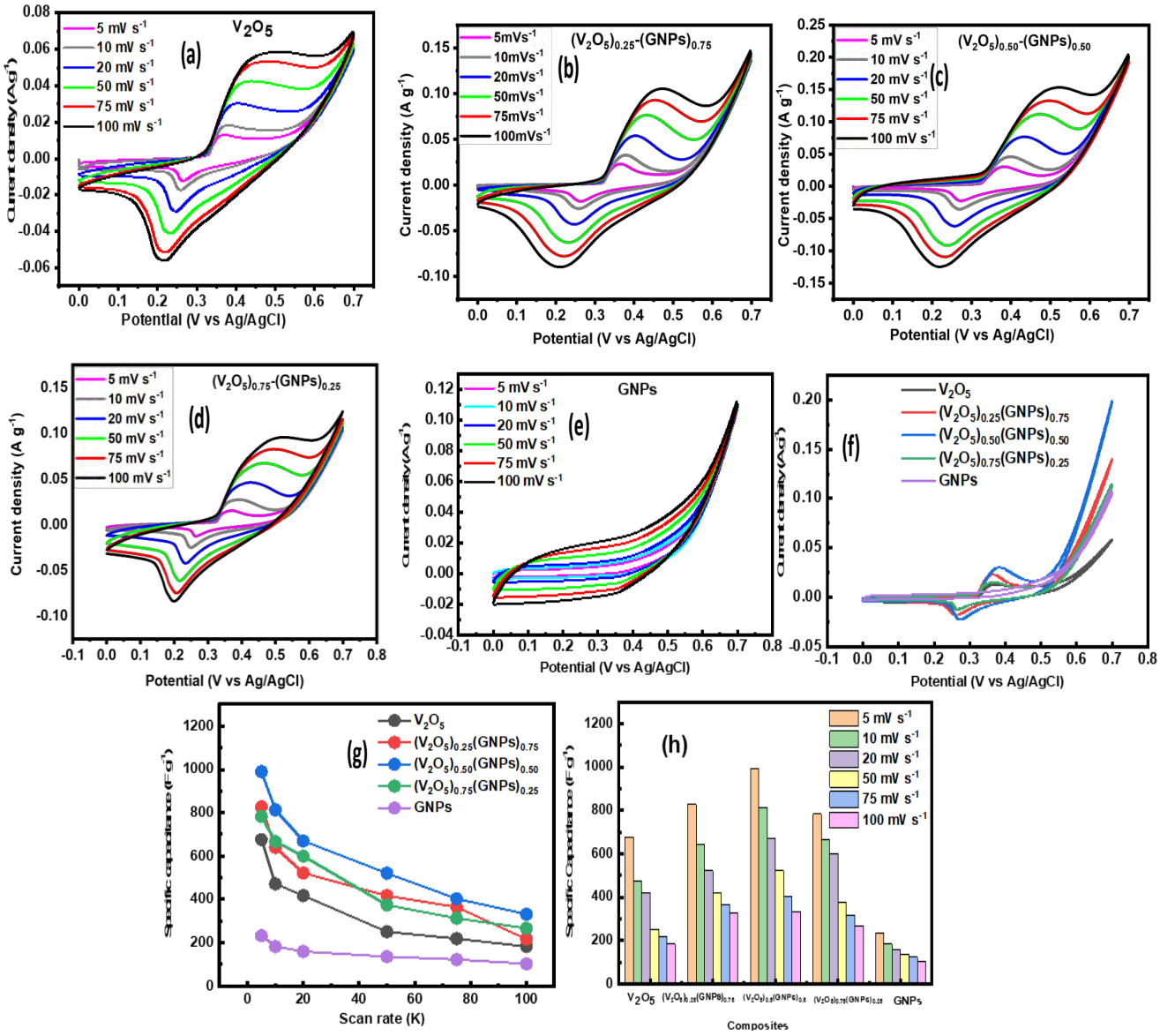

Figure 4.6: Cyclic Voltametery curves of a) V_2O_5 b) $(V_2O_5)_{0.25}(GNPs)_{0.75}$ c) $(V_2O_5)_{0.50}(GNPs)_{0.50}$ (d) $(V_2O_5)_{0.75}(GNPs)_{0.25}$ e) GNPs f) Comparison in composites current density g) Specific capacitance as a function of Scan rate h) Graphical comparison of C_{sp} at different scan rates

The outcomes show that adding GNPs can greatly improve the performance of V_2O_5 supercapacitors. Increased surface area and porosity may cause the working electrode to become more charged, which would raise the Cs values. The usage of $(V_2O_5)_{0.50}(GNPs)_{0.50}$ NCs may be useful in the creation of high-performance supercapacitors due to their high specific capacitance values. The values that are presented are greater than those for these materials that have been

published in the literature [94]. These findings are very significant and can be encouraging for the development of supercapacitors.

4.4.2 Galvano Static Charge Discharge (GCD)

The prepared $(V_2O_5)_{1-x}(GNPs)_x$ NCs have been subjected to Galvanostatic Charge Discharge (GCD) tests using different current densities (2 A/g, 4 A/g, 6 A/g, 8 A/g, and 10 A/g) in a medium of 2M NaOH electrolyte. In ordered to understand the charge and discharge mechanism, a three-electrode configuration system was used with current windows (2 A/g, 4 A/g, 6 A/g, 8 A/g, and 10 A/g) and potential windows (0.0 to 0.5V). Figure 4.7 depicts the trend of the charge-discharge mechanism, which exhibits a pseudocapacitor trend with low internal resistance, demonstrating the effectiveness of the mechanism. Equation (4.5) is used to calculate specific capacitance (Cs), and it is observed that Cs value is increased with increasing graphene content and lowering current densities as shown in the table 4.3. The specific capacitance often rises as the current density decreases. This happens because at lower current densities, ion diffusion is facilitated, and the porous structure of the electrode may be accessed. Slower processes enable ions to enter the material more deeply, lowering electrolyte resistance and the effects of polarization [95]. As a result, the electrode's surface area is used more effectively, improving the efficiency of energy storage and discharge, and raising the specific capacitance values. The Cs values of V_2O_5, $(V_2O_5)_{0.25}(GNPs)_{0.75}$, $(V_2O_5)_{0.50}(GNPs)_{0.50}$, $(V_2O_5)_{0.75}(GNPs)_{0.25}$ and GNPs are recorded 471 F/g, 486 F/g, 800 F/g, 421 F/g, and 196 F/g respectively, at the current density of 2 A/g, which is produced the greatest Cs value. This leds to greater charge accumulating at the working electrode. The high conductivity of graphene is a further factor in increasing the conductivity of the nanocomposite. Graphene has a high electrical conductivity because of its unique electronic structure, which allows electrons to pass through the material with minimal resistance. The nanocomposite's overall conductivity is increased due to the high conductivity of graphene, which creates a channel for electrons to pass through it.

Table 4.3. Specific capacitance values obtained from Cyclic charge discharge (GCD).

Current density	**Specific capacitance (Cs) F/g**				
A/g	**V_2O_5**	**$(V_2O_5)_{0.25}(GNPs)_{0.75}$**	**$(V_2O_5)_{0.5}(GNPs)_{0.5}$**	**$(V_2O_5)_{0.75}(GNPs)_{0.25}$**	**GNPs**
2A/g	471.3	486.77	800	421.68	196.64
4A/g	236.69	426.35	672	316.48	159.3
6A/g	160.05	354.99	612	270.86	142.27
8A/g	132.96	310.08	576	232.55	128.99
10A/g	92.41	271.31	340	218.87	110.85

Equations (4.6) and (4.7) were used to compute the energy density and power density of the all the NCs.

$$\boldsymbol{Cs = I\frac{\Delta t}{V}} \quad (4.5)$$

$$\boldsymbol{Eg = \frac{1}{2}Cs\,\Delta V^2} \quad (4.6)$$

$$\boldsymbol{Pg = \frac{Eg}{\Delta t}} \quad (4.7)$$

Where, (C) specific capacitance, potential window (ΔV), and time during the discharge process (Δt) [96]. The calculated energy density values of the $V_2O_5)_{0.50}(GNPs)_{0.50}$ is (Eg=27.72 Wh/Kg) and power density (Pg= 1800 W/Kg) as shown in the table 4.3. The results have been plotted as the Ragone plot, which described the relationship between energy density and power density of a different composite shown in Figure 4.7(f) This result is quite significant and novel for the supercapacitor industry and also higher than the reported data in literature of these materials [97]. A particular potential drop, often referred to as an ohmic drop or an IR drop, is associated with the inherent resistance of the electrode material is shown in the figure 4.7(g). As the current density increases, the IR drop starts to grow and reaches its maximum at 2 Ag-1. The IR drops for $(V_2O_5)1$-x(GNPs)x nanocomposites (where x = 1, 0.75, 0.50, 0.25, 0) are 0.053 Ω, 0.032 Ω, 0.0267 Ω, 0.029 Ω, and 0.0096 Ω, respectively. it is clear that the $(V_2O_5)_{0.50}(GNPs)_{0.50}$ sample

has the smallest IR decrease. Better Csp is produced by less IR drop because electrolyte ions may penetrate the material more readily.

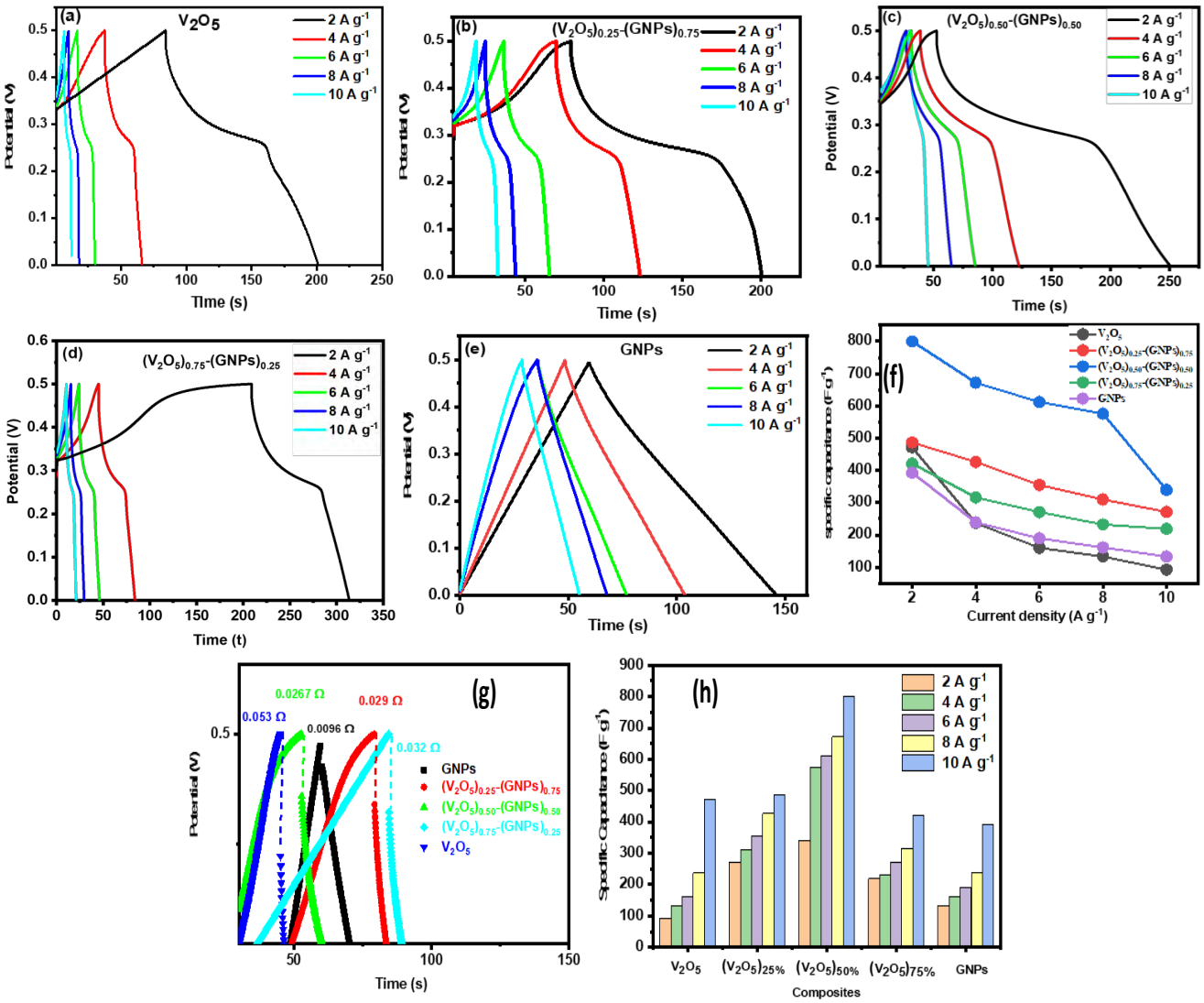

Figure 4.7: Charge discharge curves of a) V_2O_5 b) $(V_2O_5)_{0.25}(GNPs)_{0.75}$ c) $(V_2O_5)_{0.50}(GNPs)_{0.50}$ d) $(V_2O_5)_{0.75}(GNPs)_{0.25}$ e) GNPs (f) Specific capacitance Vs Current density (g) IR drop of a different composite h) Graphical comparison of C_{sp} at different Current density

The results indicate that V_2O_5 supercapacitors can perform significantly better with the addition of GNPs in matrix. Among these the high value of energy density and power density of the $V_2O_5)_{0.50}(GNPs)_{0.50}$ NCs, is very novel in the development of high-performance

supercapacitors. The values are higher than those for these materials in previous report [98]. These results are quite significant and may show promise for the supercapacitor field.

4.4.3 Electrochemical Impedance Spectroscopy (EIS)

The electrochemical Impedance Spectroscopy (EIS) has been conducted using a three-electrodes configuration system in a medium of 2M NaOH electrolyte with a frequency range of 1.0-100,000 Hz. The results of the Nyquist plots for different concentrations of $(V_2O_5)1-x(GNPs)x$ (x= 1, 0.75, 0.5, 0.25, 0) shown in Figure 4.8 reveal that the equivalent series resistance (ESR) values decrease with increasing concentration of graphene up to 50%.

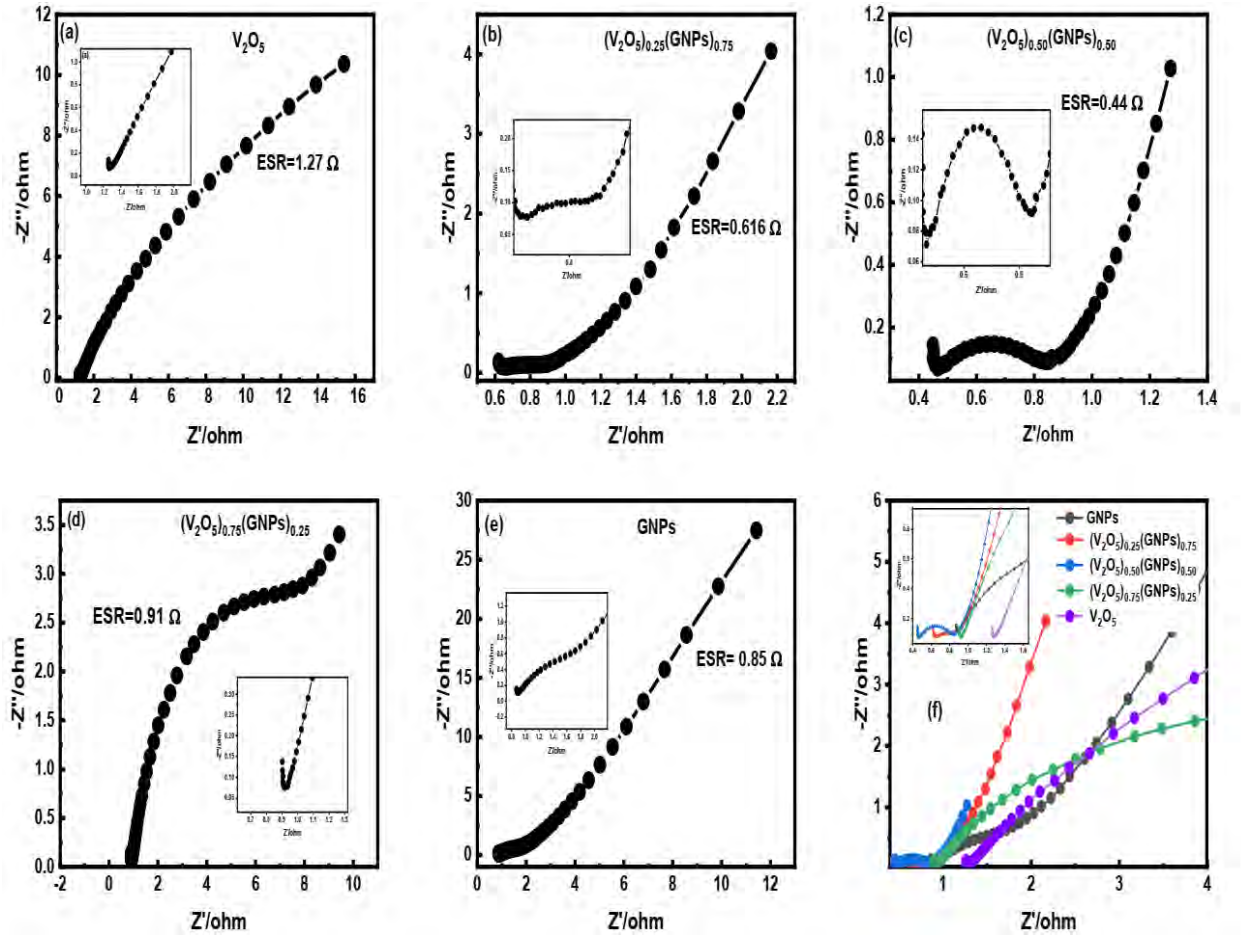

Figure 4.8: Electrochemical Impedance Spectroscopy of a) V_2O_5 b) $(V_2O_5)_{0.25}(GNPs)_{0.75}$ c) $(V_2O_5)_{0.50}(GNPs)_{0.50}$ d) $(V_2O_5)_{0.75}(GNPs)_{0.25}$ e) GNPs

The values of ESR are found to be 1.27 Ω, 0.91 Ω, 0.44 Ω, 0.616 Ω, and 0.85 Ω for $(V_2O_5)1\text{-}x(GNPs)x$ (x= 1, 0.75, 0.5, 0.25, 0) respectively. The lowest ESR value of 0.44 Ω was observed for 50% GNPs substituted NCs, indicating an enhancement in electronic conductivity and a slight reduction in cell resistance. These results are consistent with the CV and GCD observations. The Nyquist plots show a semi-circle in $(V_2O_5)_{0.50}(GNPs)_{0.50}$ as shown in the figure 4.8 (c). The semi-circle's diameter represents the charge transfer resistance or reaction kinetics at the electrode-electrolyte interface, while the frequency at which it intersects the real axis gives information about the system's internal diffusion processes, indicative of a Pseudocapacitance, as well as a 45º short line representing a Warburg element in the equivalent circuit as depict in pure V_2O_5 and GNPs. Impedance deviates from the x-axis with increasing frequency, suggesting pseudocapacitive contributions from reversible redox processes at the electrode-electrolyte interface. Both the real and imaginary parameters increase as a result, resulting in more charge storage capacity. Our results are consistent with those of our electrochemical studies and Transti analysis. The $(V_2O_5)_{0.50}(GNPs)_{0.50}$ electrode has much better electrochemical behavior than all other compositions, according to EIS results, which are strongly supported by reduced solution resistance Rs, better electrolyte ion penetration due to their lower equivalent series resistance (ESR).

4.5 Cycle Stability and Coulombic Efficiency

In order to check the stability of the device, put the device through continuous charge-discharge experiments for up to 1350 cycles in a medium of 2 Mole of NaOH electrolyte. The cycling tests were done at a current density of 2 A g-1. The best stability is shown by $(V_2O_5)_{0.50}(GNPs)_{0.50}$ (96%), followed by $(V_2O_5)_{0.75}(GNPs)_{0.25}$ (79%), GNPs (74%), and V_2O_5 (74%) in Figure 4.9. V_2O_5 shows poor cyclic stability, and which is reported in previous report [99]. Notably, $(V_2O_5)_{0.50}(GNPs)_{0.50}$ outperformed the others in terms of cycle stability. By examining the cycle stability data, it can be concluded that adding GNPs to the composite electrodes enhanced stability. Because of its outstanding mechanical and electrical conductivity GNPs can strengthen the structural integrity of the electrode material, preventing degradation and enhancing cycling efficiency. Additionally, the synergistic interactions between vanadium oxide and GNPs may lead to greater stability when combined than when used separately.

The result depicts stable coulombic efficiency for all the NCs, with $(V_2O_5)_{0.50}(GNPs)_{0.50}$ attaining the maximum efficiency of 99%. V_2O_5 has achieved the second-highest efficiency at

97%, followed by GNPs at 96%, and $(V_2O_5)_{0.75}$-$(GNPs)_{0.25}$ at 94%. $(V_2O_5)_{0.50}$-$(GNPs)_{0.50}$ exhibits a higher Coulombic efficiency, it is likely that the composite composition has a major impact on how effectively charge and discharge processes occur. Vanadium oxide may promote reversible redox processes in the composites, resulting in effective charge storage and utilization. To boost Coulombic efficiency, the GNPs component can operate as a conductive network and minimize unfavorable side effects. It is important to note that increasing Coulombic efficiency is desirable to improve supercapacitors' overall energy storage capacity and utilization.

The findings of this study show that, in comparison to the other composite, the electrode of $(V_2O_5)_{0.50}(GNPs)_{0.50}$ has greater Cycle stability and Coulombic efficiency. These results for $(V_2O_5)_{0.50}(GNPs)_{0.50}$ depict a potential use in high-performance supercapacitors. To further enhance the overall performance of supercapacitors, future research should concentrate on refining the composite composition, examining various electrode materials, and looking into additional performance measures.

Figure 4.9: Cycle stability and Coulombic efficiency of a V_2O_5 based nanocomposites

4.6 Transite analysis

The CV investigations further revealed that the redox reaction is a diffusion-controlled process, suggesting that this is likely the primary reason for the pseudocapacitive behavior observed with higher scan rates. The two differentiation approaches the Trasatti method and the Dunn method have then been used to study the diffusion-controlled faradaic and non-diffusion-controlled battery-type processes of the synthesized electrodes.. The power law $Ip=av^b$ in the Dunn technique is given by the peak current (Ip) is a function of the scan rate (V). The 'b' value is determined by the linear fit slope values. A diffusion-controlled faradaic process has a value of b=0.5, whereas a process that is not diffusion-controlled because of surface redox reactions has a value of b=1 [100]. The Trasatti approach is the simplest to explain the electrode's mechanism of the two examined methods. The linear fit of Specific capacitance (Cs) is a function of inverse square root of scan rate ($V^{-1/2}$) and Cs^{-1} is a function of square root of scan rate $V^{1/2}$ for all samples are depicted in Fig. 4.10.

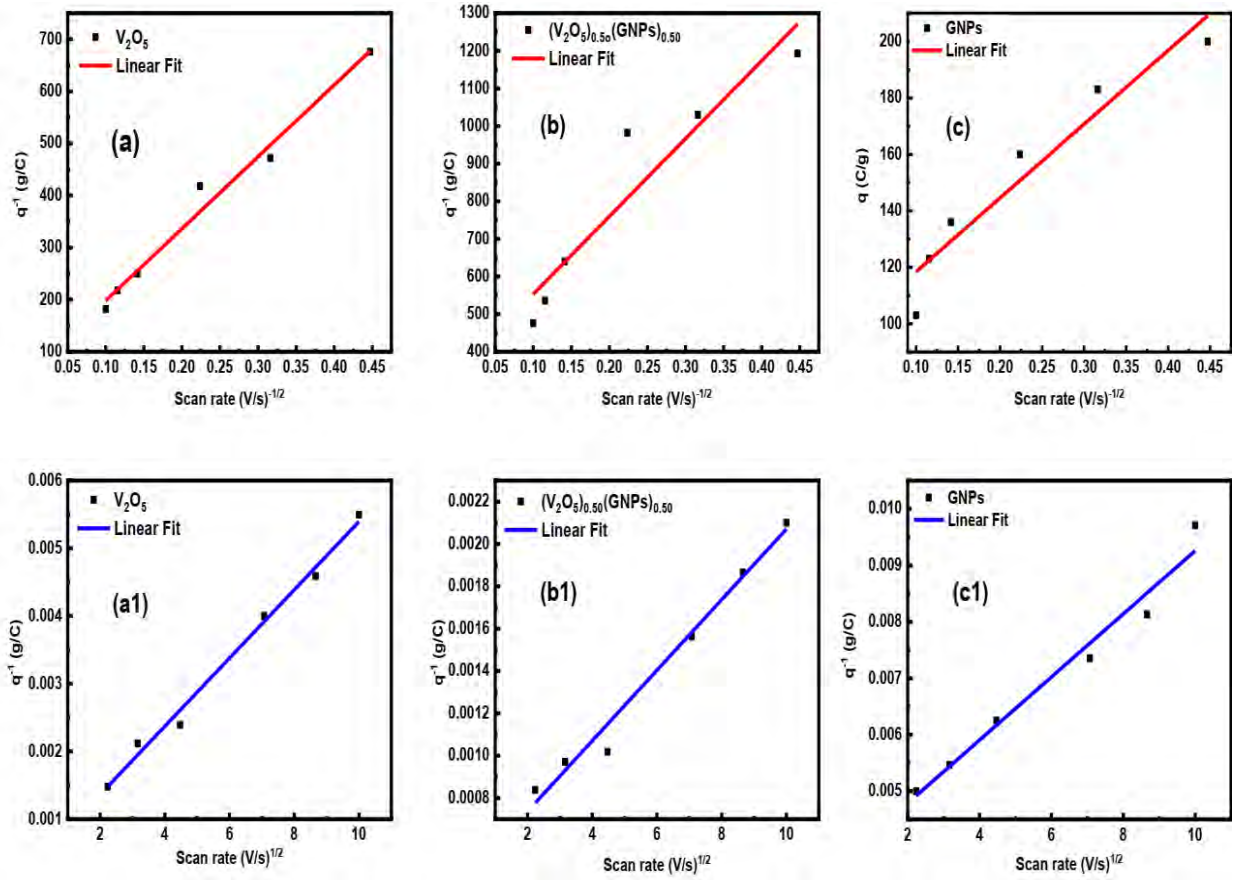

Figure 4.10: (a and a1), (b and b1), and (c and c1) Linear fits of C_s as a function of $V^{-1/2}$, and C^{-1} as a function $V^{1/2}$ for all composites

In Fig. 4.10 displays the unique capacities of V_2O_5, $(V_2O_5)_{0.25}(GNPs)_{0.75}$, $(V_2O_5)_{0.50}(GNPs)_{0.50}$, $(V_2O_5)_{0.75}(GNPs)_{0.25}$, and GNPs samples along with their EDLC (capacitive) and pseudocapacitive (diffusive) behaviors. The V_2O_5 sample had capacities of 28% and 72% generated from EDLC and PC contributions, while $(V_2O_5)_{0.25}(GNPs)_{0.75}$ had capacities of 58% and 42% derived from EDLC and PC contributions, $(V_2O_5)_{0.50}(GNPs)_{0.50}$ had capacities of 58% and 42% for EDLC and PC, $(V_2O_5)_{0.75}(GNPs)_{0.25}$ had capacities of 60% and 40% derived from EDLC and PC contributions, and GNPs had capacities of 69% and 31% for EDLC and PC as shown in the figure 4.11. In conclusion, V_2O_5 provides high energy density due to its strong PC behavior, while GNPs prioritize rapid charge/discharge cycles with their EDLC characteristics. Hybrid materials offer a compromise between these two aspects, offering a balance between energy and power density.

Figure 4.12: Percentage of Capacitive (EDLC) and Diffusive (PC)

Conclusions

In this work, V_2O_5-GNPs nanocomposites have been prepared via low effective and facile, chemical methods. The synthesized nanocomposites have shown pure crystal structures with a small variation in the lattice parameters, bond lengths, bond angles, unit cell size, unit cell volume, macro strains, and dislocations attributed to various concentrations of graphene compositions with various host matrix crystal lattice characteristics. The development of crystalline V_2O_5-GNPs nanocomposites with certain flaws has been confirmed by structural analyses. The band gap energy of V_2O_5-GNPs nanocomposites has been tuned and successfully shifted towards the visible region. This decrease in bang gap energy in V_2O_5-GNPs composites is seen as a result of crystal structural defects. The synthesized samples can be employed successfully as supercapacitor electrode material, according to electrochemical studies. The pseudocapacitive behavior of the samples has been observed, with specific capacitances of 1193 F/g and 800 F/g for $(V_2O_5)_{0.50}(GNPs)_{0.50}$ composites, respectively, at a scan rate of 5 mV/s from CV and GCD at a current density 2 A/g. This increase in specific capacitance is due to the structural voids in Vanadium oxide being highly oxidized, their better electronic conductivity, and the greater surface area accessible for charge buildup at working electrodes, presence of strain, oxygen vacancies and quantum confinement. According to electrochemical impedance spectroscopy, the composites of $(V_2O_5)_{0.50}(GNPs)_{0.50}$ have the lowest ESR value of 0.44 Ω. This could be brought on by electronic conductivity and high charge carrier flow rate. The results of this study demonstrate that electrode $(V_2O_5)_{0.50}(GNPs)_{0.50}$, has superior cycle stability and Coulombic efficiency than the other composite electrodes. The outcomes show the potential for $(V_2O_5)_{0.50}(GNPs)_{0.50}$ in high-performance supercapacitors. The Transite analysis of V_2O_5 sample had capacities of 28% and 72% generated from EDLC and PC contributions, while $(V_2O_5)_{0.25}(GNPs)_{0.75}$ had capacities of 58% and 42% derived from EDLC and PC contributions, $(V_2O_5)_{0.50}(GNPs)_{0.50}$ had capacities of 58% and 42% for EDLC and PC, $(V_2O_5)_{0.75}(GNPs)_{0.25}$ had capacities of 60% and 40% derived from EDLC and PC contributions, and GNPs had capacities of 69% and 31% for EDLC and PC. To further enhance the overall performance of supercapacitors, future research should concentrate on refining the composite composition, examining various electrode materials, and looking into additional performance measures.

Reference

[1]. Pacheco-Torgal F, Cabeza LF, Labrincha J, De Magalhaes AG. Eco-efficient construction and building materials: life cycle assessment (LCA), eco-labelling and case studies. woodhead Publishing; **2014** Feb 14.

[2]. Russell AW. Improving legitimacy in nanotechnology policy development through stakeholder and community engagement: forging new pathways. Review of policy research. **2013** Sep;30(5):566-87.

[3]. Freestone I, Meeks N, Sax M, Higgitt C. The Lycurgus cup—a roman nanotechnology. Gold bulletin. **2007** Dec;40:270-7..

[4]. Shao Y, El-Kady MF, Wang LJ, Zhang Q, Li Y, Wang H, Mousavi MF, Kaner RB. Graphene-based materials for flexible supercapacitors. Chemical Society Reviews. **2015**;44(11):3639-65.

[5]. Hassanpour M. Evaluation of Iranian electronic products manufacturing industries using an unsupervised model, ARAS, SAW, and DEA models. Journal of Industrial Engineering and Management Studies. **2019** Dec 1;6(2):1-24.

[6]. Ly K, Kellaris N, McMorris D, Johnson BK, Acome E, Sundaram V, Naris M, Humbert JS, Rentschler ME, Keplinger C, Correll N. Miniaturized circuitry for capacitive self-sensing and closed-loop control of soft electrostatic transducers. Soft Robotics. **2021** Dec 1;8(6):673-86.

[7]. Huang X, Li Y, Acharya AB, Sui X, Meng J, Teodorescu R, Stroe DI. A review of pulsed current technique for lithium-ion batteries. Energies. **2020** May 13;13(10):2458.

[8]. Kötz R, Carlen MJ. Principles and applications of electrochemical capacitors. Electrochimica acta. **2000** May 3;45(15-16):2483-98.

[9]. Stoller MD, Park S, Zhu Y, An J, Ruoff RS. Graphene-based ultracapacitors. Nano letters. **2008** Oct 8;8(10):3498-502.

[10]. Conway, B.E., Electrochemical supercapacitors: scientific fundamentals and technological applications. **2013**: Springer Science & Business Media.

Vangari, M., T. Pryor, and L.J.J.O.E.E. Jiang, Supercapacitors: Review of Materials. **2013**. 2: p. 72-79.

[11]. Goodenough, J.B. (**2007**) *Basic Research Needs for Electrical Energy Storage*, http://web.anl.gov/energy-storagescience/publications/EES_rpt.pdf

[12]. Yu A, Chabot V, Zhang J. Electrochemical supercapacitors for energy storage and delivery: fundamentals and applications. Taylor & Francis; **2013**.

[13]. Miller JR, Burke A. Electrochemical capacitors: challenges and opportunities for real-world applications. The electrochemical society interface. **2008** Mar 1;17(1):53.

[14]. Zhang, L.L. and Zhao, X.S. (**2009**) Carbon-based materials as supercapacitor electrodes. *Chemical Society Reviews*, **38** (9), 2520–2531

[15]. Purkait T, Kamboj N, Das M, Sarkar S, De Sarkar A, Dey RS. Electrochemically customized assembly of a hybrid xerogel material via combined covalent and non-covalent conjugation chemistry: an approach for boosting the cycling performance of pseudocapacitors. Journal of materials chemistry A. **2020**;8(14):6740-56.

[16]. Simon P, Gogotsi Y. Materials for electrochemical capacitors. Nature materials. **2008** Nov;7(11):845-54.

[17]. Zhu Y, Murali S, Stoller MD, Ganesh KJ, Cai W, Ferreira PJ, Pirkle A, Wallace RM, Cychosz KA, Thommes M, Su D. Carbon-based supercapacitors produced by activation of graphene. science. **2011** Jun 24;332(6037):1537-41.

[18]. González A, Goikolea E, Barrena JA, Mysyk R. Review on supercapacitors: Technologies and materials. Renewable and sustainable energy reviews. **2016** May 1;58:1189-206.

[19]. Stoller MD, Park S, Zhu Y, An J, Ruoff RS. Graphene-based ultracapacitors. Nano letters. **2008** Oct 8;8(10):3498-502.

[20]. Andreas HA, Conway BE. Examination of the double-layer capacitance of an high specific-area C-cloth electrode as titrated from acidic to alkaline pHs. Electrochimica Acta. **2006** Sep 15;51(28):6510-20.

[21]. Jalal NI, Ibrahim RI, Oudah MK. A review on Supercapacitors: Types and components. InJournal of Physics: Conference Series **2021** Aug 1 (Vol. 1973, No. 1, p. 012015). IOP Publishing.

[22]. Halper MS, Ellenbogen J. C-Supercapacitors: A brief overview, The MITRE Corporation, McLean. Virginia, Technical report 06-0667; **2006** Mar.

[23]. Malak A, Fic K, Lota G, Vix-Guterl C, Frackowiak E. Hybrid materials for supercapacitor application. Journal of Solid State Electrochemistry. **2010** May;14:811-6.

[24]. Wu ZS, Ren W, Wang DW, Li F, Liu B, Cheng HM. High-energy MnO2 nanowire/graphene and graphene asymmetric electrochemical capacitors. ACS nano. **2010** Oct 26;4(10):5835-42.

[25]. Fan Z, Yan J, Wei T, Zhi L, Ning G, Li T, Wei F. Asymmetric supercapacitors based on graphene/MnO2 and activated carbon nanofiber electrodes with high power and energy density. Advanced Functional Materials. **2011** Jun 21;21(12):2366-75.

[26]. Naoi K, Simon P. New materials and new configurations for advanced electrochemical capacitors. The Electrochemical Society Interface. **2008** Mar 1;17(1):34.

[27]. Galiński M, Lewandowski A, Stępniak I. Ionic liquids as electrolytes. Electrochimica acta. **2006** Aug 15;51(26):5567-80.

[28]. Jin Z, Yan X, Yu Y, Zhao G. Sustainable activated carbon fibers from liquefied wood with controllable porosity for high-performance supercapacitors. Journal of Materials Chemistry A. **2014**;2(30):11706-15.

[29]. Chen Q, Hu Y, Hu C, Cheng H, Zhang Z, Shao H, Qu L. Graphene quantum dots–three-dimensional graphene composites for high-performance supercapacitors. Physical Chemistry Chemical Physics. **2014**;16(36):19307-13.

[30]. Béguin F, Presser V. a. Balducci and E. Frackowiak. Adv. Mater. **2014**;2219.F.

[31]. Conway BE. Electrochemical supercapacitors: scientific fundamentals and technological applications. Springer Science & Business Media; **2013** Apr 17.

[32]. Pognon G, Brousse T, Demarconnay L, Bélanger D. Performance and stability of electrochemical capacitor based on anthraquinone modified activated carbon. Journal of Power Sources. **2011** Apr 15;196(8):4117-22.

[33]. Ruiz V, Blanco C, Granda M, Santamaría R. Enhanced life-cycle supercapacitors by thermal treatment of mesophase-derived activated carbons. Electrochimica Acta. **2008** Dec 30;54(2):305-10.

[34]. Lu M. Supercapacitors: materials, systems, and applications. John Wiley & Sons; **2013** Apr 2.

[35]. Ruiz V, Blanco C, Granda M, Santamaría R. Enhanced life-cycle supercapacitors by thermal treatment of mesophase-derived activated carbons. Electrochimica Acta. **2008** Dec 30;54(2):305-10.

[36]. Wang DW, Li F, Yin LC, Lu X, Chen ZG, Gentle IR, Lu GQ, Cheng HM. Nitrogen-doped carbon monolith for alkaline supercapacitors and understanding nitrogen-induced redox transitions. Chemistry–A European Journal. **2012** Apr 23;18(17):5345-51.

[37]. Prakash R, Shanmugam S. Electrochemical Behavior of Carbon Nanostructured Electrode Material for Supercapacitor Application. InElectrochemical Society Meeting Abstracts 226 **2014** Aug 5 (No. 3, pp. 161-161). The Electrochemical Society, Inc.

[38]. Lang JW, Yan XB, Liu WW, Wang RT, Xue QJ. Influence of nitric acid modification of ordered mesoporous carbon materials on their capacitive performances in different aqueous electrolytes. Journal of Power Sources. **2012** Apr 15;204:220-9.

[39]. Wang C, Sun L, Zhou Y, Wan P, Zhang X, Qiu J. P/N co-doped microporous carbons from H_3PO_4-doped polyaniline by in situ activation for supercapacitors. Carbon. **2013** Aug 1;59:537-46.

[40]. TIAN Y, YAN JW, XUE R, YI BL. Influence of electrolyte concentration and temperature on the capacitance of activated carbon. Acta Physico-Chimica Sinica. **2011** Feb 15;27(2):479-85.

[41]. TIAN Y, YAN JW, XUE R, YI BL. Influence of electrolyte concentration and temperature on the capacitance of activated carbon. Acta Physico-Chimica Sinica. **2011** Feb 15;27(2):479-85.

[42]. Su L, Gong L, Lü H, Xü Q. Enhanced low-temperature capacitance of MnO_2 nanorods in a redox-active electrolyte. Journal of Power Sources. **2014** Feb 15;248:212-7.

[43]. Wang X, Yuan A, Wang Y. Supercapacitive behaviors and their temperature dependence of sol–gel synthesized nanostructured manganese dioxide in lithium hydroxide electrolyte. Journal of Power Sources. **2007** Oct 25;172(2):1007-11.

[44]. Zheng JP. The limitations of energy density of battery/double-layer capacitor asymmetric cells. Journal of the Electrochemical Society. **2003** Feb 28;150(4):A484.

[45]. Wang YG, Wang ZD, Xia YY. An asymmetric supercapacitor using RuO_2/TiO_2 nanotube composite and activated carbon electrodes. Electrochimica Acta. **2005** Sep 30;50(28):5641-6.

[46]. Long JW, Bélanger D, Brousse T, Sugimoto W, Sassin MB, Crosnier O. Asymmetric electrochemical capacitors—Stretching the limits of aqueous electrolytes. Mrs Bulletin. **2011** Jul;36(7):513-22.

[47]. Huangfu C, Liu Z, Zhou Q, Wang L, Wei T, Qiu Z, Zhang S, Fan Z. Covalent grafting of p-phenylenediamine molecules onto a “bubble-like” carbon surface for high performance asymmetric supercapacitors. Journal of Materials Chemistry A. **2020**;8(4):1767-78.

[48]. Torchała K, Kierzek K, Machnikowski J. Capacitance behavior of KOH activated mesocarbon microbeads in different aqueous electrolytes. Electrochimica Acta. **2012** Dec 30;86:260-7.

[49]. Wu H, Wang X, Jiang L, Wu C, Zhao Q, Liu X, Yi L. The effects of electrolyte on the supercapacitive performance of activated calcium carbide-derived carbon. Journal of power sources. **2013** Mar 15;226:202-9.

[50]. Bichat MP, Raymundo-Piñero E, Béguin F. High voltage supercapacitor built with seaweed carbons in neutral aqueous electrolyte. Carbon. **2010** Dec 1;48(15):4351-61.

[51]. Demarconnay L, Raymundo-Piñero E, Béguin F. A symmetric carbon/carbon supercapacitor operating at 1.6 V by using a neutral aqueous solution. Electrochemistry Communications. **2010** Oct 1;12(10):1275-8.

[52]. Kuo SL, Wu NL. Investigation of pseudocapacitive charge-storage reaction of $MnO_2 \cdot nH_2O$ supercapacitors in aqueous electrolytes. Journal of The Electrochemical Society. **2006** May 9;153(7):A1317.

[53]. Xu C, Wei C, Li B, Kang F, Guan Z. Charge storage mechanism of manganese dioxide for capacitor application: Effect of the mild electrolytes containing alkaline and alkaline-earth metal cations. Journal of Power Sources. **2011** Sep 15;196(18):7854-9.

[54]. Li S, Qi L, Lu L, Wang H. Cotton-assisted preparation of mesoporous manganese oxide for supercapacitors. RSC advances. **2012**;2(17):6741-3.

[55]. Long JW, Bélanger D, Brousse T, Sugimoto W, Sassin MB, Crosnier O. Asymmetric electrochemical capacitors—Stretching the limits of aqueous electrolytes. Mrs Bulletin. **2011** Jul;36(7):513-22.

[56]. Azaïs P, Duclaux L, Florian P, Massiot D, Lillo-Rodenas MA, Linares-Solano A, Peres JP, Jehoulet C, Béguin F. Causes of supercapacitors ageing in organic electrolyte. Journal of power sources. **2007** Sep 27;171(2):1046-53.

[57]. Galiński M, Lewandowski A, Stępniak I. Ionic liquids as electrolytes. Electrochimica acta. **2006** Aug 15;51(26):5567-80.

[58]. El-Kady MF, Strong V, Dubin S, Kaner RB. Laser scribing of high-performance and flexible graphene-based electrochemical capacitors. Science. **2012** Mar 16;335(6074):1326-30.

[59]. Liu C, Li F, Ma LP, Cheng HM. Advanced materials for energy storage. Advanced materials. **2010** Feb 23;22(8):E28-62.

[60]. Yan J, Wang Q, Wei T, Fan Z. Recent advances in design and fabrication of electrochemical supercapacitors with high energy densities. Advanced Energy Materials. **2014** Mar;4(4):1300816.

[61]. Peres, N. and R.M.J.N.J.o.P. Ribeiro, *Focus on graphene.* **2009**. **11**(9): p. 095002

[62]. Yang G, Li L, Lee WB, Ng MC. Structure of graphene and its disorders: a review. Science and technology of advanced materials. **2018** Dec 31;19(1):613-48.

[63]. Choi W, Lahiri I, Seelaboyina R, Kang YS. Synthesis of graphene and its applications: a review. Critical Reviews in Solid State and Materials Sciences. **2010** Feb 11;35(1):52-71.

[64]. Jiménez-Suárez, A. and S.J.A.S. Prolongo, *Graphene nanoplatelets*. **2020**, MDPI. p. 1753.

[65]. Wang G, Zhang L, Zhang J. A review of electrode materials for electrochemical supercapacitors. Chemical Society Reviews. **2012**;41(2):797-828.

[66]. Yu G, Hu L, Vosgueritchian M, Wang H, Xie X, McDonough JR, Cui X, Cui Y, Bao Z. Solution-processed graphene/MnO_2 nanostructured textiles for high-performance electrochemical capacitors. Nano letters. **2011** Jul 13;11(7):2905-11.

[67]. Chellan P, Sadler PJ. The elements of life and medicines. Philosophical Transactions of the Royal Society A: Mathematical, Physical and Engineering Sciences. **2015** Mar 13;373(2037):20140182.

[68]. Uchaker E, Zheng YZ, Li S, Candelaria SL, Hu S, Cao GZ. Better than crystalline: amorphous vanadium oxide for sodium-ion batteries. Journal of Materials Chemistry A. **2014**;2(43):18208-14.

[69]. Miyazaki H, Matsuura T, Ota T. Vanadium oxide-based photochromic composite film. RSC advances. **2017**;7(5):2388-91.

[70]. Zhang Y, Huang Y. Facile synthesis and characterization of rough surface V_2O_5 nanomaterials for pseudo-supercapacitor electrode material with high capacitance. Bulletin of Materials Science. **2017** Oct;40:1137-49.

[71]. Dhand C, Dwivedi N, Loh XJ, Ying AN, Verma NK, Beuerman RW, Lakshminarayanan R, Ramakrishna S. Methods and strategies for the synthesis of diverse nanoparticles and their applications: a comprehensive overview. Rsc Advances. **2015**;5(127):105003-37.

[72]. Almessiere MA, Slimani Y, Rehman S, Khan FA, Polat EG, Sadaqat A, Shirsath SE, Baykal A. Synthesis of Dy-Y co-substituted manganese-zinc spinel nanoferrites induced anti bacterial and anti-cancer activities: Comparison between sonochemical and sol-gel auto combustion methods. Materials Science and Engineering: C. **2020** Nov 1;116:111186.

[73]. Zhang S, Li L, Kumar A. Materials characterization techniques. CRC press; **2008** Dec 22.

[74]. Rasoulis M, Vernardou D. Electrodeposition of vanadium oxides at room temperature as cathodes in lithium-ion batteries. Coatings. **2017** Jul 12;7(7):100.

[75] He BB. Two-dimensional X-ray Diffraction. John Wiley & Sons; **2018** May 18.

[76]. M. Prześniak-Welenc, J. Karczewski, J. Smalc-Koziorowska, M. Łapiński, W. Sadowski, B. Kościelska. *RSC Adv.* **2016**, *6*, 55689-55697.

[77]. Rasul S, Alazmi A, Jaouen K, Hedhili MN, Costa PM. Rational design of reduced graphene oxide for superior performance of supercapacitor electrodes. Carbon. **2017** Jan 1;111:774-81.

[78]. Vandenabeele P. Practical Raman spectroscopy: an introduction. John Wiley & Sons; **2013** Jul 3. & Sons.

[79]. Sur UK. Surface-enhanced Raman spectroscopy: recent advancement of Raman spectroscopy. Resonance. **2010** Feb;15(2):154-64.

[80]. Vandenabeele P. Practical Raman spectroscopy: an introduction. John Wiley & Sons; **2013** Jul 3.

[81]. Desai R, Mankad V, Gupta SK, Jha PK. Size distribution of silver nanoparticles:UVvisible spectroscopic assessment. Nanoscience and nanotechnology letters. **2012** Jan 1;4(1):30-4.

[82]. Clark BJ, Frost T, Russell MA, editors. UV Spectroscopy: Techniques, instrumentation and data handling. Springer Science & Business Media; **1993** Apr 30.

[83]. Akhtar K, Khan SA, Khan SB, Asiri AM. Scanning electron microscopy: Principle and applications in nanomaterials characterization. Handbook of materials characterization. **2018**:113-45.

[84]. Trinosky PA, Wells L. Implementation of ANSI 13.36-Radiation Safety Training for Workers.

Lawrence Livermore National Lab.(LLNL), Livermore, CA (United States); **2000** Nov 18.

[85]. Waelder J, Vasquez R, Liu Y, Maldonado S. A description of the faradaic current in cyclic voltammetry of adsorbed redox species on semiconductor electrodes. Journal of the American Chemical Society. **2022** Apr 1;144(14):6410-9.

[86]. Boukhalfa S, Evanoff K, Yushin G. Atomic layer deposition of vanadium oxide on carbon nanotubes for high-power supercapacitor electrodes. Energy & Environmental Science. **2012**;5(5):6872-9.

[87]. Wang H, Robinson JT, Li X, Dai H. Solvothermal reduction of chemically exfoliated graphene sheets. Journal of the American Chemical Society. **2009** Jul 29;131(29):9910-1.

[88]. Li M, Sun G, Yin P, Ruan C, Ai K. Controlling the formation of rodlike V_2O_5 nanocrystals on reduced graphene oxide for high-performance supercapacitors. ACS applied materials & interfaces. **2013** Nov 13;5(21):11462-70.

[89]. Kumar A, Singh P, Kulkarni N, Kaur D. Structural and optical studies of nanocrystalline V2O5 thin films. Thin Solid Films. **2008** Jan 30;516(6):912-8.

[90]. Shahzad W, Badawi AK, Rehan ZA, Khan AM, Khan RA, Shah F, Ali S, Ismail B. Enhanced visible light photocatalytic performance of Sr0. 3 (Ba, Mn) 0.7 ZrO_3 perovskites anchored on graphene oxide. Ceramics International. **2022** Sep 1;48(17):24979-88.

[91]. Nagaraju DH, Wang Q, Beaujuge P, Alshareef HN. Two-dimensional heterostructures of V_2O_5 and reduced graphene oxide as electrodes for high energy density asymmetric supercapacitors. Journal of Materials Chemistry A. **2014**;2(40):17146-52.

[93]. Sangamithirai D, Ramanathan S. Electrochemical sensing platform for the detection of nitroaromatics using g-C_3N_4/V_2O_5 nanocomposites modified glassy carbon electrode. Electrochimica Acta. **2022** Dec 1;434:141308.

[94]. Zhang, Yifu, Jiqi Zheng, Yunfeng Zhao, Tao Hu, Zhanming Gao, and Changgong Meng. "Fabrication of V_2O_5 with various morphologies for high-performance electrochemical capacitor." *Applied Surface Science* 377 (**2016**): 385-393.

[95]. Zhang D, Yan T, Shi L, Peng Z, Wen X, Zhang J. Enhanced capacitive deionization performance of graphene/carbon nanotube composites. Journal of Materials Chemistry. **2012**;22(29):14696-704.

[96]. Zeng, Zifan, Dengzhi Wang, Jiliang Zhu, Fuqiang Xiao, Yudong Li, and Xiaohong Zhu. "NiCo 2 S 4 nanoparticles//activated balsam pear pulp for asymmetric hybrid capacitors." *CrystEngComm* 18, no. 13 (**2016**): 2363-2374.

[97]. H. Liu, W. Zhu, D. Long, J. Zhu, G. Pezzotti, Porous V_2O_5 nanorods/reduced graphene oxide composites for high performance symmetric supercapacitors, Appl. Surf. Sci. 478 (**2019**) 383–392.

[98]. Zhang, Yifu, Jiqi Zheng, Yunfeng Zhao, Tao Hu, Zhanming Gao, and Changgong Meng. "Fabrication of V_2O_5 with various morphologies for high-performance electrochemical capacitor." *Applied Surface Science* 377 (**2016**): 385-393.

[99]. Li Y, Yao J, Uchaker E, Zhang M, Tian J, Liu X, Cao G. Sn-doped V_2O_5 film with enhanced lithium-ion storage performance. The Journal of Physical Chemistry C. **2013** Nov 14;117(45):23507-14.

[100]. Isacfranklin, M., Rathinam Yuvakkumar, G. Ravi, Dhayalan Velauthapillai, Mehboobali Pannipara, and Abdullah G. Al-Sehemi. "Superior supercapacitive performance of Cu 2 MnSnS 4 asymmetric devices." *Nanoscale Advances* 3, no. 2 (**2021**): 486-498.